Engineering Geology 197 (2015) 253–266

Contents lists available at ScienceDirect

Engineering Geology

journal homepage: www.elsevier.com/locate/enggeo

Development of magnitude-bound relations for paleoliquefaction analyses: New Zealand case study

B.W. Maurer [a], R.A. Green [a], M.C. Quigley [b,c], S. Bastin [c]

[a] Department of Civil and Environmental Engineering, Virginia Tech, Blacksburg, VA, USA
[b] School of Earth Sciences, University of Melbourne, Melbourne, Australia
[c] Department of Geological Sciences, University of Canterbury, Christchurch, New Zealand

ARTICLE INFO

Article history:
Received 4 March 2015
Received in revised form 18 August 2015
Accepted 19 August 2015
Available online 18 September 2015

Keywords:
Paleoliquefaction
Earthquake
Magnitude bound curve
Liquefaction
New Zealand
Christchurch

ABSTRACT

Magnitude-bound relations are often used to estimate paleoearthquake magnitudes from paleoliquefaction data. This study proposes New Zealand-based magnitude-bound curves that are developed using (a) liquefaction field observations and (b) a newly proposed back-calculation approach that combines the simplified liquefaction evaluation procedure with a regionally appropriate ground motion prediction equation. For (b) both deterministic and probabilistic frameworks are proposed. The magnitude bound curves back-calculated using either the deterministic or probabilistic frameworks are advantageous in that they can be used to predict the spatial distribution of liquefaction in regions where historical liquefaction field observations are limited or poorly documented, and because soil- and site-specific conditions can be incorporated into magnitude-bound analyses. Moreover, curves developed using the probabilistic framework allow for the range of possible causative earthquake magnitudes to be better understood and quantified. To demonstrate the use of the proposed relations, paleoliquefaction features discovered in eastern Christchurch (NZ) are analyzed. The 1869 ~M_w4.8 Christchurch earthquake and/or 1717 ~M_w8.1 Alpine Fault earthquake are found to be the most likely candidates amongst known historical and paleoearthquakes for triggering liquefaction over the permissible time range (ca. 1660 to 1905 A.D.). This study demonstrates the potential of the proposed magnitude-bound curves to provide insight in to past, present, and future hazards, proving their utility even in cases of limited evidence. The approach of developing and applying magnitude bound curves proposed herein is not limited to parts of New Zealand, but rather, can be applied worldwide.

1. Introduction

In regions experiencing infrequent moderate-to-large earthquakes, the historic record may be insufficient to provide accurate inputs for seismic hazard analyses because (1) some active faults may be historically seismically quiescent and not easily identifiable from surface evidence, thereby posing an unspecified potential earthquake source, and (2) seismic phenomena such as liquefaction and rockfall may pose a potential hazard but may not have occurred historically. The 2010–2011 Canterbury earthquake sequence (CES) in New Zealand provided a powerful demonstration of these limitations. The CES involved at least 7 damaging earthquakes sourced from at least 12 faults (Beavan et al., 2012) that were previously unidentified and historically seismically quiescent. As many as ten distinct episodes of liquefaction (Quigley et al., 2013) and five distinct episodes of rockfall (Mackey and Quigley, 2014) occurred at some sites in the mainshock (M_w 7.1 Darfield earthquake) and largest aftershocks (e.g., 2011 M_w 6.2 Christchurch earthquake, 185 fatalities). Approximately 75% of buildings within the central business district (CBD) of Christchurch required demolition or extensive repair (Kam et al., 2011). Due to extensive liquefaction-induced land and infrastructure damage, more than 6000 residential properties in eastern Christchurch were purchased by the central government (http://cera.govt.nz/residential-red-zone) at a post-insurance pay out loss exceeding $NZ 1 b ($US 800 m) (Parker and Steenkamp, 2012).

Pre-CES seismic hazard models for the region (e.g., Stirling et al., 2007) that combined regional active faults (source models) with 'floating' unidentified sources (distributed seismicity) indicated that (a) proximal, moderate M_w earthquakes from unidentified distributed sources (including blind faults) contributed the largest seismic shaking hazard to Christchurch, (b) earthquakes up to M_w 7.2 on unidentified sources beneath the Canterbury Plains west of Christchurch were possible, and (c) expected return times of potentially liquefaction-inducing peak ground accelerations (PGA ~0.1 to 0.2 g) for class C (shallow soil) site conditions ranged from ca. 50 to 200 yr. However, prior to the CES, none of this data had been seriously validated with rigorous paleoseismic investigations in Christchurch. The occurrence of a highly damaging series of earthquakes sourced from previously unknown and primarily blind faults highlighted the inherent incompleteness of source-based seismic hazard catalogs, demonstrating the necessity for geologic studies of prehistoric phenomena such as rockfalls (Mackey and Quigley, 2014) and liquefaction features (Bastin et al., 2015) to

http://dx.doi.org/10.1016/j.enggeo.2015.08.023
0013-7952/

supplement seismic hazard models and predict the impacts of future earthquakes. Despite a wealth of recent paleoliquefaction studies in Christchurch (e.g., Almond et al., 2012; Quigley et al., 2013; Bastin et al., 2015; Maurer et al., 2014; Villamor et al., 2014), a significant challenge remains in understanding the spatial distribution of earthquake sources and shaking intensities that induced paleo-liquefaction, and are thus capable of inducing future liquefaction, in this region.

Paleoliquefaction studies have two phases. The first phase entails the performance of field investigations, wherein paleoliquefaction features are located, mapped, and dated. The reader is referred to Obermeier et al. (2001, 2005) for broad overviews of paleoliquefaction field investigation, and to the intensive investigations by Obermeier and Dickenson (2000), Tuttle (2001), Talwani and Schaeffer (2001), Cox et al. (2004), and Tuttle et al. (2002a, 2002b, 2005) for specific case studies. The second phase, and the focus of this study, is back-analysis, wherein quantitative techniques are used to determine the magnitude of the causative paleoearthquake and better constrain its source location. Specifically, this study aims to advance the state of the art in back-analysis techniques so that the results of field investigation can be used to accurately assess the paleoseismic history of a region to the extent possible.

Back-analysis techniques have been increasingly applied in paleoliquefaction studies in many seismically active regions (e.g., Obermeier, 1998; Tuttle, 2001; Talwani and Schaeffer, 2001; Cox et al., 2004; Green et al., 2005; Bastin et al., 2015). While several techniques have been proposed for estimating earthquake magnitudes from paleoliquefaction data, one of the more credible and widely-used is the "magnitude-bound" procedure (e.g., Obermeier, 1998; Olson et al., 2005a, 2005b; Papathanassiou et al., 2005; Pirrotta et al., 2007; Tuttle and Hartleb, 2012). This approach uses correlations relating earthquake magnitude to the site-to-source distance of the most distal observation of liquefaction. Developed from observations in modern earthquakes, these correlations are commonly referred to as magnitude-bound curves. Fig. 1 presents several such correlations for a variety of geographic and tectonic settings (Kuribayashi and Tatsuoka, 1975; Ambraseys, 1988; Papadopoulos and Lefkopoulos, 1993; Wakamatsu, 1993; Galli, 2000; Aydan et al., 2000; Papathanassiou, 2005; Pirrotta et al., 2007; Castilla and Audemard, 2007), where site-to-source distance is quantified in terms of epicentral distance (Fig. 1a) and the distance to most proximal fault rupture (Fig. 1b). The position of these curves, which bound the most distal liquefaction features, is inherently a function of earthquake source characteristics (e.g., rupture mechanism), transmission characteristics (e.g., ground motion attenuation and site effects), and liquefaction susceptibility (e.g., soil state and gradation, and ground water depth). Because these factors vary regionally, region-specific correlations provide more accurate estimates than those developed from global data (Obermeier et al., 2001; Olson et al., 2005a, 2005b).

In addition, inherent to these curves are differing criteria for data inclusion, including the quality and extent of field study, the certainty of earthquake source location and magnitude (e.g., instrumental vs. macroseismic), the style of faulting and focal depth, and the overall anomalousness of data. For example, in developing his curves, Ambraseys (1988) did not consider (1) deep-focus earthquakes, which produce more distal liquefaction than shallow crustal earthquakes; or (2) anomalous cases that would bias the maximum site-to-source distance of liquefaction, including those where conditions greatly enhanced liquefaction susceptibility, such as irrigated fields or sloping ground. Conversely, Castilla and Audemard (2007) included both deep-focus earthquakes and anomalous cases in developing their correlation from global data. For example, Castilla and Audemard (2007) include data from the 1977 M_w7.5 Bucharest, Romania earthquake, having a focal depth of 91–110 km (Ambraseys, 1988; Berg et al., 1980), as well

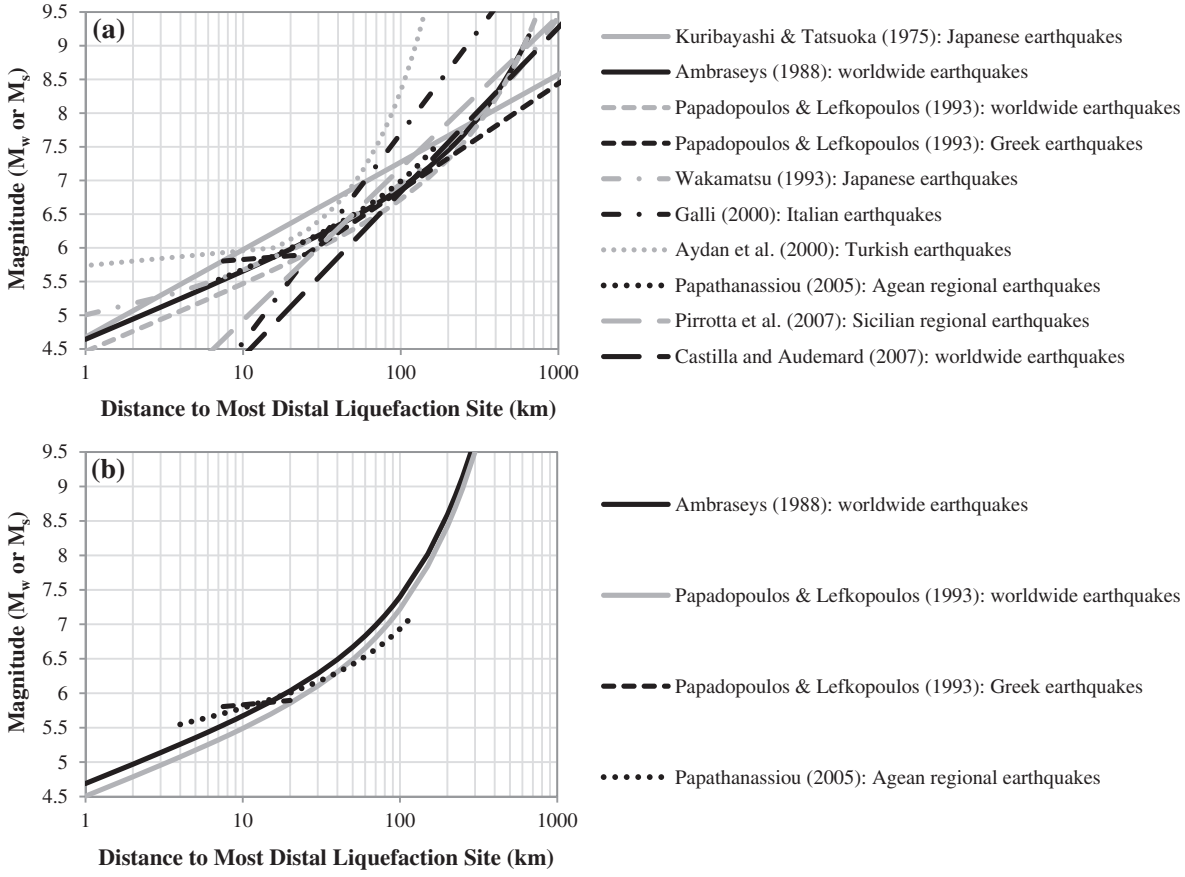

Fig. 1. Magnitude-bound curves for various geographic and tectonic settings, where site-to-source distance is quantified in terms of (a) epicentral distance and (b) closest distance to fault rupture.

as data from aftershocks following the 1989 M_w5.9 Bova del Tocuyo, Venezuela and M_w6.9 Loma Prieta, USA earthquakes. While further research is needed, it has been shown that surface manifestations of liquefaction may be observed at greater site-to-source distances during aftershocks than in equivalent-magnitude mainshocks, possibly due to increased liquefaction susceptibility from reduced aging-effects, or to the presence of existing liquefaction dikes, which act as conduits between liquefied strata and the ground surface (Green et al., 2013; Maurer et al., 2014). Due to the inclusion of this data, and as shown in Fig. 1a, the Castilla and Audemard (2007) correlation estimates a significantly lower magnitude at shorter site-to-source distances, as compared to using correlations proposed by other authors. Importantly, differing criteria for data selection can result in significant differences to magnitude-bound curves. Therefore, in addition to using regionally-appropriate correlations, familiarity with the provenance of a magnitude-bound curve is critical; to place derivative results in proper context, a user must be aware of a correlation's source data, development, and caveats for use.

While magnitude-bound curves specific to New Zealand have not yet been proposed, there is a clear and present need. In light of the prior inconspicuousness of local faults and the exceedance of design ground-motions during the CES, there is a need to reassess the magnitude-recurrence rates of earthquakes local to Christchurch. Preliminary evidence suggests liquefaction-inducing earthquakes occurred between A.D. 1000 and A.D. 1400 (Villamor et al., 2014) and between AD 1660 – 1803 and ca. 1905 (Bastin et al., 2015) in distinct parts of Christchurch, however the origins of these earthquakes are unknown. The penultimate earthquake on the source of the Darfield earthquake (Greendale Fault) occurred ca. 20–30 kyr ago (Hornblow et al., 2014) and rock fall evidence suggests that no large earthquakes have occurred on the local faults responsible for the 2011 February M_w6.2 and June M_w6.0 Christchurch earthquakes within the last 6000 to 8000 years (Mackey and Quigley, 2014), indicating that the CES sources were not responsible for the paleoliquefaction. Region-specific magnitude-bound curves could thus assist in the interpretation of such evidence and help to elucidate the region's paleoseismic history. As such, the objectives of this study are to: (1) develop a NZ-based magnitude-bound curve using the traditional approach of using modern liquefaction field observations; (2) develop NZ-based magnitude-bound curves using a newly proposed back-calculation approach using the simplified liquefaction evaluation procedure in conjunction with a regionally appropriate ground motion prediction equation (GMPE); and (3) demonstrate the use of these curves by analyzing paleoliquefaction features recently discovered in Christchurch. It is hoped that these correlations ultimately aid in more accurately assessing the regional seismic hazard.

2. Development of NZ-based magnitude-bound curves

Two approaches are used to develop NZ-based magnitude-bound curves for shallow crustal earthquakes. The first is the traditional approach using modern liquefaction field observations (e.g., Ambraseys, 1988), but based on data from earthquakes in New Zealand only. The second is a newly proposed back-calculation approach using the simplified liquefaction evaluation procedure in conjunction with a regionally appropriate GMPE. In this latter approach both deterministic and probabilistic frameworks are used; these frameworks are described in detail. Lastly, discrepancies between the curves developed using the two approaches are discussed, and recommendations are made for use in New Zealand.

2.1. Magnitude-bound curves based on field observations

The magnitude-bound curves shown in Fig. 1 were all developed using field liquefaction observations. In each case, the site-to-source distances of the most distal liquefaction features were compiled from modern earthquakes with known magnitudes. While exceptional cases exist, nearly all magnitude-bound curves in the literature are constructed to bound the compiled data, rather than provide a best fit of the data. Consequently, magnitude-bound curves almost always give a lower-bound estimate of magnitude, rather than a median estimate. To demonstrate, the magnitude-bound curves of Ambraseys (1988) are plotted in Fig. 2 for epicentral distance (R_{epi}) and "fault distance," the latter being similar to Joyner-Boore distance (R_{jb}) as measured by Ambraseys (1988); the data used to develop these correlations are also plotted. It can be seen that using either distance metric (i.e., R_{epi} or ~R_{jb}), the proposed magnitude-bound curves are drawn to bound the respective datasets. As such, these relations give the minimum earthquake magnitude expected to induce liquefaction at any given site-to-source distance.

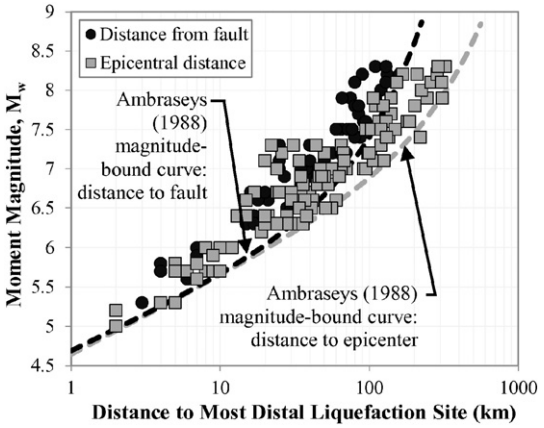

Fig. 2. Magnitude-bound relations for epicentral distance (R_{epi}) to most distal liquefaction site, and distance from fault (~R_{jb}) to most distal liquefaction site, using global data (Ambraseys, 1988); global data from earthquakes with liquefaction observations, as compiled by Ambraseys (1988), are also plotted.

Following in the style of Ambraseys (1988) and many others, data from historic shallow crustal earthquakes in New Zealand with documented liquefaction observations are herein compiled. As summarized in Table 1, there are at least 20 such events. While some of these historic earthquakes are also found in the Ambraseys (1988) database, the estimated magnitude and/or site-to-source distance of liquefaction are in most cases updated using recent refinements from the literature. For example, the 1848 Marlborough, New Zealand earthquake is listed in the Ambraseys (1988) database as having a surface wave magnitude of M_s7.1, derived from macroseismic data. More recently, Mason and Little (2006) reinvestigated the rupture length and displacement of the Awatere Fault during the Marlborough earthquake and proposed a refined moment magnitude estimate of M_w7.4 to M_w7.7. Since this event contributes to the positioning of the magnitude-bound curve, refinement of the estimated magnitude is significant. Many other events in Table 1 have never before been compiled for use in magnitude-bound correlations. In some cases, the earthquake magnitude and/or source location are uncertain; for these cases, published values from the literature are given in Table 1 along with the value(s) deemed most credible and selected for inclusion in our development of a NZ-based correlation. For compatibility with prior studies, fault distance as compiled in Table 1 is the measured R_{jb}, though the more general label is also retained in consideration of the many uncertainties inherent to a paleoliquefaction study (e.g., varying focal depths and mechanisms).

In addition to the exclusionary rules proposed by Ambraseys (1988), cases were omitted from the database for the following reasons: (1) several aftershock events from the CES were omitted because the most distal liquefaction was observed at a site of prior recent liquefaction; as discussed previously, including these events could bias the maximum site-to-source distance of liquefaction; and (2) observations of liquefaction in reclaimed land (e.g., liquefaction induced in the Port of Wellington by the 2013 Cook Strait and Lake Grassmere earthquakes) were omitted because the liquefaction susceptibility of artificial fills

Table 1
Historic earthquakes in New Zealand with liquefaction observations.

Date	Earthquake	Estimated M[a]	Reference	Plotted M	Estimated R_{epi} (km)[d]	Estimated R_{jb} (km)[e]	Reference	Plotted R_{epi} (km)	Plotted R_{jb} (km)
16 Oct. 1848	Marlborough	7.1[b]	Fairless and Berrill (1984); Ambraseys (1988)	7.5	128	–	Fairless and Berrill (1984)	128	–
		7.4–7.7	Mason and Little (2006)		126	–	Ambraseys (1988)		
23 Jan. 1855	Wairarapa	7.6	Ambraseys (1988)	8.2	175	–	Fairless and Berrill (1984)	230	153
		8.2	Hancox (2005)		168	132	Ambraseys (1988)		
		8.2–8.3	GeoNet (2015)		230	153	Hancox (2005)		
31 Aug. 1888	N. Canterbury	7.0[c]	Fairless and Berrill (1984)	7.1	50	45	Ambraseys (1988)	50	45
		6.9	Ambraseys (1988)		50	–	Fairless and Berrill (1984)		
		7.0–7.3	GeoNet (2015)						
15 Nov. 1901	Cheviot	7.0	Fairless and Berrill (1984)	6.9	69	–	Fairless and Berrill (1984)	65	40
		7.3[b]	Ambraseys (1988)		65	40	Ambraseys (1988)		
		6.9 ± 0.2[b]	Dowrick and Smith (1990)						
		7.1–7.5	Berrill et al. (1994)						
		6.8[c]	GeoNet (2015)						
22 Feb. 1913	Westport	6.8[c]	De Lange and Healy (1986)	6.8	27	–	Fairless and Berrill (1984)	27	–
25 Dec. 1922	Motunau	6.5	Doser and Robinson (2002)	6.5	40	–	Christensen (2001), after Stirling et al. (1999)	40	–
		6.4[c]	GeoNet (2015)						
9 Mar. 1929	Arthur's Pass	6.9[b]	Fairless and Berrill (1984)	7.0	36	–	Fairless and Berrill (1984)	36	–
		6.9[b]	Ambraseys (1988)		35	–	Ambraseys (1988)		
		7.0	GeoNet (2015)						
17 Jun. 1929	Murchison	7.8[b]	Fairless and Berrill (1984); Carr and Berrill (2004)	7.8	122	117	Carr and Berrill (2004), after Benn (1992)	122	117
3 Feb. 1931	Hawke's Bay	7.9[c]	Fairless and Berrill (1984)	7.8	140	–	Fairless and Berrill (1984)	140	85
		7.7	Ambraseys (1988)		140	85	Ambraseys (1988)		
		7.8[b]	GeoNet (2015)						
24 Jun. 1942	Wairarapa	7.0[c]	Fairless and Berrill (1984)	7.1	63	–	Fairless and Berrill (1984)	63	55
		6.9	Ambraseys (1988)		63	55	Ambraseys (1988)		
		6.9–7.2	GeoNet (2015)						
24 May 1968	Inangahua	7.0[c]	Fairless and Berrill (1984)	7.1	34	25	Ambraseys (1988)	30.6	23.7
		7.1	Ambraseys (1988)		30.6	23.7	Carr and Berrill (2004)		
		7.1	Anderson et al. (1994)						
2 Mar. 1987	Edgecumbe	6.5	GeoNet (2015)	6.5	18	13	Franks (1988)	18	13
4 June 1988	Te Anau	6.7	GeoNet (2015)	6.7	46	–	Reyners et al. (2003)	46	–
28 Jan. 1991	Hawks Craig	6.2[c]	Carr and Berrill (2004)	5.9	18	–	Carr and Berrill (2004)	18	–
		5.9	GeoNet (2015)						
22 Aug. 2003	Fiordland	7.2	GeoNet (2015)	7.2	84	55	Glassey (2006)	84	55
18 July 2004	L. Rotoehu	5.4	GeoNet (2015)	5.4	6.5	–	Hancox et al. (2004)	6.5	–
4 Sept. 2010	Darfield	7.1	GeoNet (2015)	7.1	64	54	Green and Cubrinovski (2010)	54	44
22 Feb. 2011	Christchurch	6.2	GeoNet (2015)	6.2	23.5	17	CGD - Canterbury Geotechnical Database (2012)	23.5	17
21 July 2013	Cook Strait	6.5	GeoNet (2015)	6.5	21	0.9	Van Dissen et al. (2013)	21	0.9
16 Aug. 2013	L. Grassmere	6.6	GeoNet (2015)	6.6	34.5	33.3	Van Dissen et al. (2013)	34.5	33.3

[a] Moment magnitude (M_w), except where noted.
[b] Surface-wave magnitude (M_s).
[c] Unknown magnitude scale.
[d] Site-to-source distance from epicenter to most distal liquefaction feature (epicentral distance, R_{epi}).
[e] Site-to-source distance from fault rupture to most distal liquefaction feature (Joyner-Boore distance, R_{jb}).

differs from that of natural deposits (e.g., Towhata et al., 2014). In addition, it is noted that two of the compiled earthquakes (1987 M_w6.5 Edgecumbe; 2004 M_w5.4 Rotoehu) occurred in the Taupo Volcanic Zone, which is known to have higher anelastic attenuation rates than other crustal regions of NZ (Bradley, 2013), and which might thus lessen the spatial distribution of liquefaction.

In Fig. 3, the database of New Zealand liquefaction observations is plotted in magnitude-bound space, as are the resulting curves for R_{epi} and R_{jb}. These magnitude-bound curves were developed by modifying the functional form of Ambraseys (1988) to better fit the New Zealand data. Although the curve based on R_{jb} is poorly constrained at small magnitudes due to limited case-history data, it is known that the maximum distance between R_{epi} and R_{jb} must converge with diminishing earthquake magnitude; the curves were thus constructed to account for this requisite convergence. The correlations based on R_{epi} and R_{jb} are respectively defined by:

$$M_w = -0.26 + 2.4 \times 10^{-7.58} \times \left(R_{epi} \times 10^{4.98}\right) + 0.96 \times \log\left(R_{epi} \times 10^{5.02}\right) \quad (1a)$$

$$M_w = -0.26 + 2.35 \times 10^{-7.58} \times \left(R_{jb} \times 10^{5.2}\right) + 0.96 \times \log\left(R_{jb} \times 10^{5.09}\right) \quad (1b)$$

where M_w is moment magnitude; and R_{epi} and R_{jb} are the site-to-source distances (km) of the most distal liquefaction observation. As is evident from Fig. 3, Eqs. (1a) and (1b) are lower-bound curves and thus yield minimum earthquake magnitude estimates; in reality the causative earthquake magnitudes could be much larger than those given by Eqs. (1a) and (1b).

2.2. Back-calculated magnitude-bound curves

As stated previously, magnitude-bound curves have historically been developed using liquefaction field observations. However, they can also be developed using the simplified liquefaction evaluation procedure in conjunction with regionally appropriate GMPEs. These "back-calculated" magnitude-bound curves will be formulated using both deterministic and probabilistic frameworks, beginning with the former. In the following, these frameworks are presented, as is the

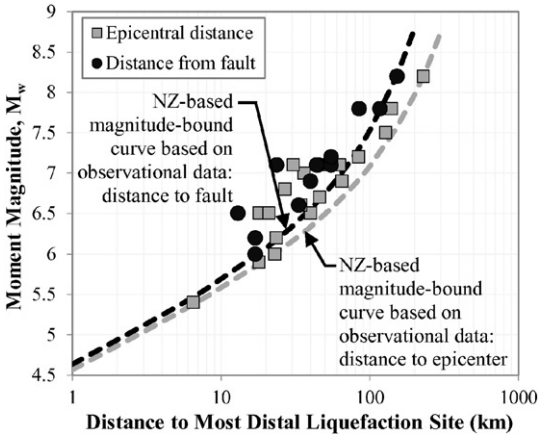

Fig. 3. Magnitude-bound relations for epicentral distance (R_{epi}) to most distal liquefaction site, and distance from fault (R_{jb}) to most distal liquefaction site, using New Zealand data (a la Ambraseys, 1988); data from historic earthquakes in New Zealand with liquefaction observations, as compiled in Table 1, are also plotted.

development of NZ-based correlations and a discussion of the assumptions used therein.

2.2.1. Framework: deterministic magnitude-bound curves

In engineering practice, the potential for earthquake-induced liquefaction is commonly assessed using the "simplified" liquefaction evaluation procedure (Whitman, 1971; Seed and Idriss, 1971). First developed for the Standard Penetration Test (SPT), the original procedure has gone through numerous updates (e.g., Seed et al., 1985; Youd et al., 2001; Cetin et al., 2004; Idriss and Boulanger, 2008; Boulanger and Idriss, 2014) and versions have been developed for the Cone Penetration Test (CPT) (e.g., Seed and DeAlba, 1986; Stark and Olson, 1995; Robertson and Wride, 1998; Moss et al., 2006; Idriss and Boulanger, 2008; Boulanger and Idriss, 2014) and shear-wave velocity (V_s) (e.g., Andrus and Stokoe, 2000; Kayen et al., 2013). In this procedure, the factor of safety against liquefaction (FS_{liq}) for level ground conditions is equal to the ratio of the cyclic resistance of the soil (CRR) to the earthquake induced cyclic stress ($CSR_{M\,=\,7.5,\sigma'\,=\,1\ atm}$, or for brevity, CSR). The CSR subscripts indicate that it is computed for an M_w7.5 earthquake and in-situ vertical effective stress (σ'_v) of 1 atm, reflecting the influence of shaking duration and overburden stress on liquefaction. To use this procedure for back-analysis at a paleoliquefaction site, the soil stratum (i.e., the "critical layer") with depth-thickness-density combination consistent with the observed liquefaction response of the site is assumed to have an FS_{liq} of 1.0 (Eq. (2)).

$$FS_{liq} = \frac{CRR}{CSR_{M=7.5,\ \sigma'_v=1\ atm}} = 1.0 \tag{2}$$

By substituting the general form of the simplified liquefaction evaluation procedure for level ground conditions (in this case, for SPT data) for CSR, the minimum peak ground acceleration required to induce liquefaction may be expressed as:

$$a_{max} = CRR\left((N_1)_{60cs}\right) \times MSF(M_w) \times K_\sigma \times \frac{g \times \sigma'_{vo}}{0.65 \times \sigma_v \times r_d} \tag{3}$$

where a_{max} = peak geometric-mean horizontal ground acceleration; $(N_1)_{60cs}$ = representative SPT blow count, normalized for overburden pressure, corrected to an equivalent energy ratio of 60%, and adjusted for fines content; MSF = magnitude scaling factor to adjust for the duration of shaking; M_w = moment magnitude; K_σ = dimensionless factor incorporating the effect of overburden pressure on liquefaction resistance; g = coefficient of acceleration due to gravity; σ'_{vo} = initial in-situ vertical effective stress; σ_v = in-situ vertical total stress; and r_d = dimensionless stress reduction factor accounting for the non-rigid response of the soil column. Olson et al. (2005a), Green et al. (2005, 2014), and Green and Olson (2015) provide guidelines for selection of critical layers and the representative in-situ parameters (i.e., $(N_1)_{60cs}$, σ'_{vo}, σ_v) required in Eq. (3); the exact form of the remaining terms depends on which version of the simplified procedure is used (e.g., Youd et al., 2001; Cetin et al., 2004; Idriss and Boulanger, 2008).

As shown in Fig. 4a, the boundary defined by Eq. (3) separates combinations of a_{max} and M_w that are sufficient to induce liquefaction from combinations that are insufficient. As there are infinitely many combinations sufficient to induce liquefaction, a regionally appropriate GMPE is used to determine credible a_{max}–M_w combinations for a given site, where the GMPE defines a_{max} as a function of earthquake magnitude (M_w) and site-to-source distance (R), amongst other factors. A GMPE is plotted in Fig. 4b (dashed line) with variable M_w and R (e.g., R_{epi}, R_{rup}, etc.) equal to the distance between the liquefaction site and provisional earthquake source location. Thus, this line represents the expected a_{max} at the liquefaction site corresponding to various causative earthquake magnitudes. As indicated in Fig. 4b, the portion of this line plotting above the boundary defined by Eq. (3) corresponds to a_{max}–M_w combinations that could induce liquefaction at the site. The intersection of the GMPE with the boundary-line (i.e., $FS_{liq} = 1$) thus defines the lower-bound a_{max}–M_w combination. In other words, this gives the minimum magnitude earthquake expected to induce liquefaction. Since both Eq. (3) and the GMPE compute a_{max} as a function of M_w, the back-calculated a_{max}–M_w solution requires iteration.

In addition to the a_{max} defined by Eq. (3), there exists a threshold shear strain (γ_t) below which excess pore pressures are not expected to develop, irrespective of the number of loading cycles (Dobry et al., 1980, 1982). In other words, there is an a_{max} below which liquefaction will not occur regardless of shaking duration (where earthquake magnitude is often used as a proxy for shaking duration), but this is not explicitly considered by the cyclic-stress framework in Eq. (3). The solution obtained from Eq. (3) is therefore contingent on this requirement, which can affect the shape of the magnitude-bound curve at far-field distances. Assuming $\gamma_t = 10^{-4}$ for sands (Dobry et al., 1980, 1982), it follows from the formulation of CSR (e.g., Seed and Idriss, 1971) that:

$$(a_{max})_t = \frac{G_{max} \times 10^{-4} \times (G/G_{max})_{\gamma_t}}{0.65 \times \sigma_v \times r_d} \tag{4}$$

where $(a_{max})_t$ = minimum peak geometric-mean horizontal ground acceleration required to induce a threshold shear strain, γ_t, of 10^{-4}; G_{max} = small-strain shear modulus; $(G/G_{max})_{\gamma t}$ = shear modulus reduction coefficient, determined at strain γ_t; and σ_v and r_d are as defined previously. $(G/G_{max})_{\gamma t}$ may be estimated from (1) shear modulus reduction curves for similar soils (e.g., Dobry et al. (1980) suggest a representative value of 0.75 for all sands); or (2) using a more refined G/G_{max} model that considers the influence of in-situ conditions on modulus reduction behavior (e.g., Ishibashi and Zhang, 1993; Darendeli, 2001). Lastly, G_{max} can be computed from small strain shear wave velocities measured in-situ or can be estimated from other in-situ test data (e.g., SPT, CPT) using one of several empirical relations (e.g., Seed et al., 1986; Rix and Stokoe, 1991). Thus, the iterative solution to develop magnitude-bound curves should also account for $(a_{max})_t$, such that the back-calculated a_{max}–M_w solution shown schematically in Fig. 4b satisfies $(a_{max})_t$.

In summary, the a_{max} required to induce liquefaction (i.e., $FS_{liq} = 1$) is computed from liquefaction triggering methodology using in-situ and dynamic soil parameters. A GMPE, which also accounts for site-response effects, is then used to determine the minimum magnitude earthquake required to induce this a_{max} at variable site-to-source distances, the cumulative result being a magnitude-bound curve.

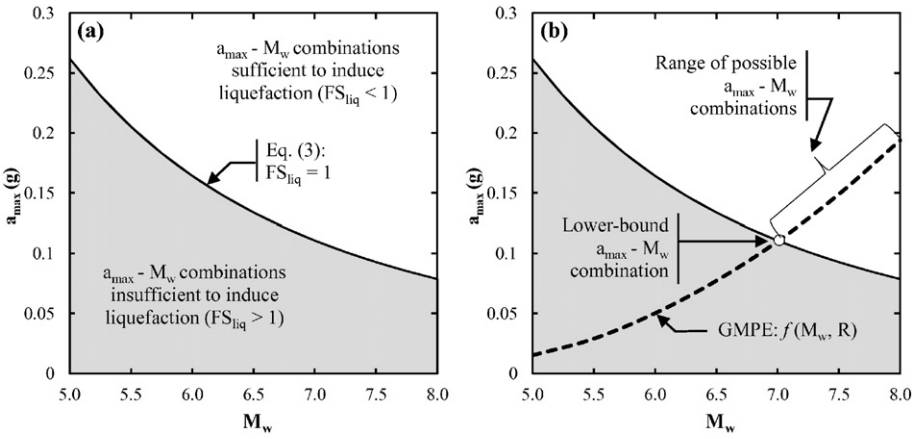

Fig. 4. (a) a_{max}-M_w combinations sufficient to induce liquefaction at a hypothetical site; and (b) credible a_{max}-M_w combinations at the same hypothetical site having site-to-source distance R, as determined by a ground motion prediction equation (GMPE).

2.2.2. Assumptions and development: deterministic magnitude bound-curves

To develop a back-calculated magnitude-bound curve which bounds all of the data points (i.e., a lower-bound curve), it should be recognized that the data controlling the location of the curve correspond to the greatest liquefaction susceptibility, the greatest seismic loading, or some combination of the two scenarios. In other words, the site-to-source distance at which liquefaction can occur increases with the presence of highly liquefiable soils and/or greater than expected seismic loading for a respective M_w and R. Thus, as seen in Figs. 2 and 3, data points plotting significantly "left" of the bounding curve (i.e., at shorter site-to-source distances) correspond to cases where either (1) lithospheric structure, the tectonic setting, source characteristics (e.g. directivity, stress drop), transmission characteristics, or aleatoric variability produce lesser ground motions; or (2) the combination of ground water depth and soil properties result in lesser liquefaction susceptibility. In light of this, a deterministic lower-bound curve is back-calculated herein using inputs corresponding to elevated liquefaction susceptibility and greater than expected seismic loading.

This lower-bound curve is generated using the Cetin et al. (2004) version of the simplified procedure to evaluate the representative soil profile shown in Fig. 5a. Collectively, these inputs (i.e., $(N_1)_{60cs}$, σ'_{vo}, σ_v) are consistent with "High" to "Very High" liquefaction susceptibility, as given by Olson et al. (2005b) and adapted from Youd and Hoose (1977) and Youd and Perkins (1978). The Cetin et al. (2004) procedure was principally chosen for its probabilistic capabilities, the benefits of which will be discussed later in this paper. However, for the purposes of developing deterministic magnitude-bound curves, the procedure is used as recommended by Cetin et al. (2004) for deterministic assessments of liquefaction potential. To account for the threshold strain (Eq. (4)), G_{max} is estimated using the Seed et al. (1986) relation for SPT data, while $(G/G_{max})_{\gamma t}$ is computed from the Darendeli (2001) model. In addition, the Bradley (2010, 2013) GMPE is utilized assuming: Site Class D (soil) conditions; a strike-slip fault for which the depth to the top of rupture (Z_{tor}) is 1 km; and median + 0.5σ a_{max}. The Bradley (2010, 2013) GMPE is a NZ-specific modification of the Chiou and Youngs (2008) model that corrects empirically identified discrepancies for New Zealand recordings, and Site Class D is a reasonable assumption for site-profiles with liquefiable soils. For example, the majority of Christchurch strong motion stations are located on Site Class D profiles (Wood et al., 2011; Wotherspoon et al., 2014). From a limited parametric analysis, the assumed focal mechanism (e.g., strike-slip vs. reverse) was found to be relatively insignificant compared to other uncertainties; the implications of the Z_{tor} assumption are discussed subsequently, following the development of the magnitude-bound curves. Lastly, because the Bradley (2010, 2013) GMPE uses distance metrics based on fault geometry (e.g., R_{jb}, R_{rup}), empirical conversions of site-to-source distance metrics (Scherbaum et al., 2004) are used to develop a magnitude-bound relation based on epicentral distance. It should be noted that while these conversions appear reasonable, they are herein used beyond suggested limits of $0 < R_{jb} < 100$ km and $5.0 < M_w < 7.5$, and as such, the validity of the resulting relation outside these limits is uncertain. With the above assumptions, and using the framework discussed previously, magnitude-bound relations for R_{epi} and R_{jb} are computed, as shown in Fig. 6a; also plotted is the database of New Zealand liquefaction observations given in Table 1. As can be seen in Fig. 6a, it is thus possible to back-calculate magnitude-bound curves consonant with field liquefaction observational data using reasonable assumptions.

While lower-bound curves help to constrain paleoseismic histories, they may also significantly underestimate the magnitudes of liquefaction-inducing paleoearthquakes. As evident from Figs. 2, 3, and 6a, the back-calculated magnitudes of some earthquakes are underestimated significantly when the most distal observation of liquefaction plots far from the magnitude-bound curve. For example, in the 1968 M_w7.1 Inangahua, New Zealand earthquake, the most distal liquefaction was observed at $R_{jb} \approx 24$ km, or $R_{epi} \approx 31$ km (using epicenter location and earthquake source dimensions from Anderson et al., 1994). Using the back-calculated curves shown in Fig. 6a, the causative earthquake magnitude is erroneously estimated to be M_w6.1 (using R_{jb}) or M_w6.2 (using R_{epi}). As such, a median or "best-estimate" magnitude could be obtained using a correlation which provides a best fit of the M_w vs. R data, in lieu of one that bounds the data. A best-estimate magnitude-bound curve can be back-calculated using input-parameters representative of median conditions. To compute such a curve, the Bradley (2010, 2013) GMPE is used to estimate the

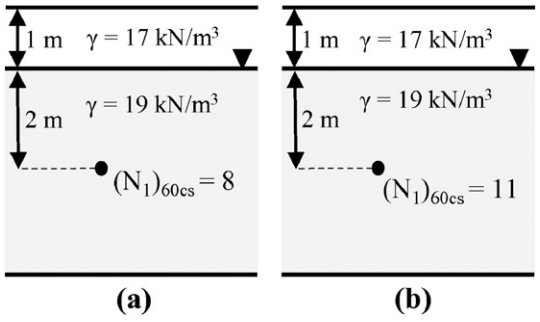

Fig. 5. Representative soil profiles used to develop deterministic (a) lower-bound; and (b) median back-calculated magnitude-bound curves, where: γ = total unit weight; $(N_1)_{60cs}$ = SPT blow count, normalized for overburden pressure, corrected to an equivalent energy ratio of 60%, and adjusted for fines content (FC). The liquefiable strata in (a) and (b) are comprised of saturated clean sands having FC < 5%.

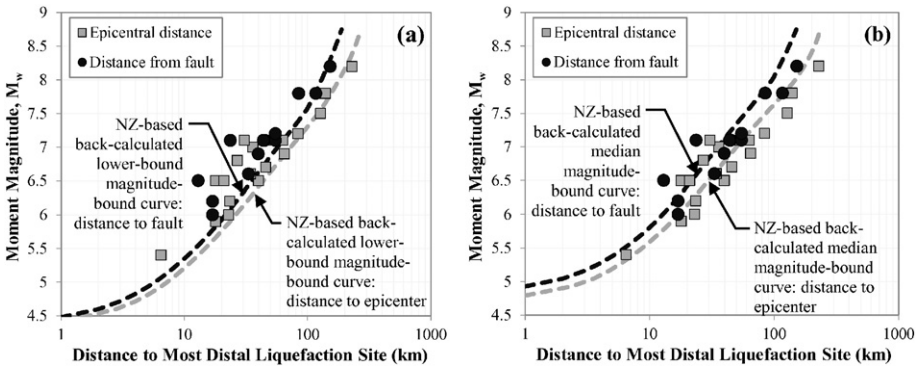

Fig. 6. Magnitude-bound relations for epicentral distance (R_{epi}) to most distal liquefaction site, and distance from fault (R_{jb}) to most distal liquefaction site, using: (a) back-calculated lower-bound approach and (b) back-calculated median approach, as described in text; data from historic earthquakes in New Zealand with liquefaction observations, as compiled in Table 1, are also plotted.

median a_{max} for the previously assumed conditions: a Class D site in a strike-slip tectonic environment with $Z_{tor} = 1$ km. In addition, the Cetin et al. (2004) procedure is used to evaluate the representative soil profile shown in Fig. 5b, characterized as having "Moderate" to "High" liquefaction susceptibility according to Olson et al. (2005b). The resulting median curves for R_{epi} and R_{jb} are shown in Fig. 6b along with the database of New Zealand liquefaction observations given in Table 1; as before, the relation based on R_{epi} is computed using the conversions of site-to-source distance metrics given by Scherbaum et al. (2004). As expected, and shown in Fig. 6b, the back-calculated median relations pass *through* the M_w vs. R data rather than bound it.

Inherent to the Bradley (2013) GMPE, and by corollary, the framework proposed herein, a value of Z_{tor} must be assumed. While nearly all $M_w \geq 7.0$ crustal earthquakes have fault ruptures that reach the ground surface, smaller magnitude earthquakes often do not, particularly those where reverse-slip is predominant (Boore, 2011). While the 4 largest events of the CES (i.e., 4 Sept. 2010 M_w7.1; 22 Feb. 2011 M_w6.2; 13 June 2011 M_w6.0; and 23 Dec. 2011 M_w6.0) all had $Z_{tor} \leq 1$ km (Beavan et al., 2012), some of the historic events compiled in Table 1 are known to have had deeper ruptures and larger Z_{tor} values. In general, as Z_{tor} increases for a given magnitude earthquake, the predicted a_{max} decreases at short R_{jb}, remains unchanged at moderate R_{jb}, and increases at long R_{jb}; accordingly, the potential for liquefaction also follows this trend. For example, if the magnitude-bound curves shown in Fig. 6a were re-developed for an increase in Z_{tor} to 5 km, the magnitude-bound curves would shift upward more than 0.1M_w for 1 km < R_{jb} < 4 km (i.e., a larger magnitude earthquake is now needed to induce liquefaction at these distances), increase less than 0.1M_w for 4 km < R_{jb} < 15 km, and decrease for R_{jb} > 15 km (i.e., a smaller magnitude earthquake is now needed to induce liquefaction at these distances), reaching a reduction of 0.17M_w at $R_{jb} = 100$ km. Consequently, the back-calculated curves may be less accurate for crustal earthquakes having greater rupture depths. The magnitude-bound curves developed herein are intended for shallow crustal earthquakes with low Z_{tor} values; the user should recognize the limitations of applying these curves to deeper ruptures, for which a separate set of curves could be developed via the proposed framework.

2.2.3. Framework: probabilistic magnitude-bound curves

The development of back-calculated, deterministic magnitude-bound curves represents a significant advancement for regions where well-documented field liquefaction observational data is not available, allowing for soil- and site-specific conditions to be incorporated in magnitude-bound analyses. However, the inputs needed in a paleoliquefaction study are uncertain, and deterministic frameworks are inherently limited insofar as accounting for this variability. A probabilistic framework could thus allow for the range of possible causative earthquake magnitudes to be better understood and quantified. Such a framework is made possible by the development of probabilistic liquefaction evaluation procedures (e.g., Cetin et al., 2004; Moss et al., 2006; Idriss and Boulanger, 2012; Boulanger and Idriss, 2014). These procedures recognize that liquefaction does not always occur when predicted by a deterministic procedure (i.e., $FS_{liq} < 1.0$). In reality, there is a probability of liquefaction (P_L) associated with every combination of cyclic-resistance and cyclic-stress. For example, the P_L-triggering curves proposed by Cetin et al. (2004) are shown in Fig. 7a; it can be seen that for a given $(N_1)_{60cs}$, P_L increases with increasing CSR. However, CSR is also uncertain due to the uncertainties of the inputs that define it (i.e., a_{max}, r_d, σ_v, σ'_{vo}). For example, the a_{max} induced by a given earthquake at a particular site-to-source distance is uncertain, as shown in Fig. 7b using the Bradley (2010, 2013) GMPE. Likewise, r_d is uncertain, as computed by the Moss et al. (2006) relation shown in Fig. 7c. Collectively, these and other uncertainties pertaining to soil/site conditions (e.g., G_{max}, threshold shear strain, penetration resistance, total stress, effective stress) appeal to the advantages of probabilistic magnitude-bound curves.

The framework proposed herein does not attempt to quantify every uncertainty entering a paleoliquefaction study, but it incorporates the most significant parameter variability and demonstrates how quantifiable uncertainties can be accounted for; additional uncertainties, if known, could be incorporated in a similar manner. Using the total probability theorem to integrate over select uncertainties, the probability that a site liquefies in an earthquake of magnitude, M, at site-to-source distance, R, can be expressed as:

$$P(\text{Site Liquefies}|\text{EQK}: M, R) = \int_{a_{max}} \int_{r_d} P(\text{Site Liquefies}|a_{max}, r_d) f(a_{max}|M, R)\, f_{r_d}(r_d) \cdot dr_d \cdot da_{max}. \quad (5)$$

In Eq. (5), the conditional probability of liquefaction P(Site Liquefies|EQK:M,R) is given by a probabilistic liquefaction evaluation procedure (e.g., Cetin et al., 2004; Moss et al., 2006; Boulanger and Idriss, 2012, 2014); the conditional probability density function f(a_{max}|M,R) is given by a GMPE; and $f_{r_d}(r_d)$ is a probability density function for r_d. As discussed previously, "simplified" liquefaction evaluation procedures do not explicitly account for the threshold strain (γ_t). The probability of an induced strain exceeding this threshold in an earthquake of magnitude, M, at site-to-source distance, R, can be expressed as:

$$P(\gamma \geq \gamma_t|\text{EQK}: M, R) = \int_{a_{max}} \int_{r_d} \int_{\frac{G}{G_{max}}} P\left(\gamma \geq \gamma_t \middle| a_{max}, r_d, \frac{G}{G_{max}}\right) f(a_{max}|M, R)\, f_{r_d}(r_d) f_{\frac{G}{G_{max}}}\left(\frac{G}{G_{max}}\right) d\frac{G}{G_{max}} \cdot dr_d \cdot da_{max}. \quad (6)$$

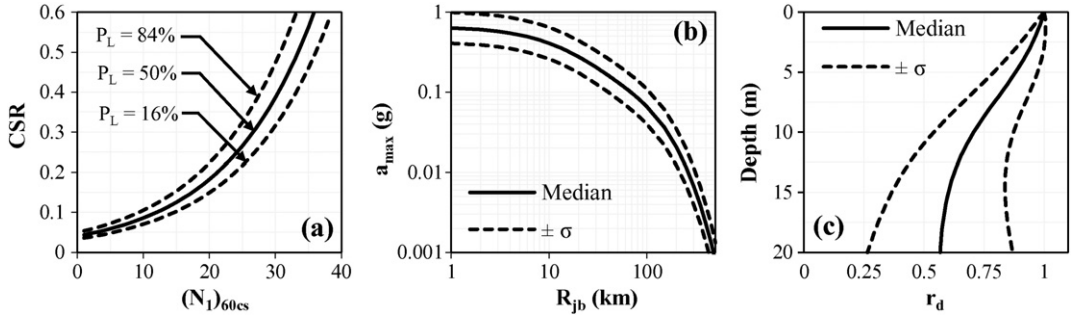

Fig. 7. Uncertainties associated with back-calculated magnitude-bound curves, to include (a) the probability of liquefaction triggering, P_L (Cetin et al., 2004); (b) ground motion prediction (Bradley, 2013); and (c) the stress reduction coefficient, r_d (Moss et al., 2006).

In Eq. (6), the conditional probability density function $f(a_{max}|M,R)$ is given a GMPE, while $f_{r_d}(r_d)$ and $f_{G/Gmax}(G/G_{max})$ are probability density functions for r_d and G/G_{max}, respectively; throughout Eq. (8) G/G_{max} refers to the modulus reduction coefficient at γ_t, defined previously (Eq. (4)) as $(G/G_{max})_{\gamma t}$. As will be demonstrated, Eqs. (7)–(8) can be used to define a suite of curves (one for each value of R considered) relating the probability of liquefaction to earthquake magnitude; from this suite of curves, probabilistic magnitude-bound curves are developed.

2.2.4. Assumptions and development: probabilistic magnitude bound-curves

For the representative soil profile shown in Fig. 5a, Eqs. (7)–(8) are used to develop probabilistic magnitude-bound curves, as follows: $P(\text{Site Liquefies}|a_{max},r_d)$ is computed using the Cetin et al. (2004) liquefaction evaluation procedure; $f(a_{max}|M,R)$ is computed from the Bradley (2010, 2013) GMPE for Site Class D conditions and a strike-slip rupture for which Z_{tor} = 1 km; r_d and f_{r_d} are computed from the Moss et al. (2006) V_s-independent r_d relation; and G/G_{max} and $f_{G/G_{max}}$ are computed from the Darendeli (2001) model. In addition, the following parameters are treated as deterministic: G_{max}, as computed by the Seed et al. (1986) relation for SPT data; γ_t, assumed to be 10^{-4}, per Dobry et al. (1980); and $(N_1)_{60cs}$, σ_v, and σ'_{vo}, as given in Fig. 5a and inspired by Olson et al. (2005b).

Applying the above assumptions to the probabilistic framework discussed previously, Eqs. (5) and (6) are each used to generate a suite of P_L vs. M_w curves for selected values of R_{jb}, as shown in Fig. 8a for Eq. (5). From these probability curves, probabilistic magnitude-bound curves are constructed, as shown in Fig. 8b for P_L values of 16% and 84% (i.e., median ± σ); it can be seen that the magnitude-bound curves are defined by Eq. (5) for small to moderate values of R_{jb}, and by Eq. (6) at long distances. Combining results from Eqs. (5) and (6), magnitude-bound curves based on R_{jb} and R_{epi} are plotted in Fig. 9a and b, respectively, for P_L values of 7%, 16%, 31%, 50%, 69%, 84%, and 93%; also plotted is the database of New Zealand liquefaction observations (Table 1) and the deterministic lower-bound and median magnitude-bound curves developed previously (Fig. 6). Once again, the curves based on R_{epi} are developed using the Scherbaum et al. (2004) empirical conversions. It can be seen in Fig. 9a and b that: (1) the deterministic lower-bound and median curves closely align with the P_L = 16% and P_L = 50% curves, respectively; and (2) the field liquefaction observational data is generally consistent with the back-calculated median ± σ prediction. Provided in an electronic supplement are data for reproducing the probabilistic curves shown in Fig. 9.

2.3. Discussion and recommendations

To investigate discrepancies amongst the proposed magnitude-bound curves, the NZ-based back-calculated curve (P_L = 16%) and lower-bound curve developed from observational data are plotted in Fig. 10 for R_{jb} (Fig. 10a) and R_{epi} (Fig. 10b); also plotted are liquefaction observations from global (Ambraseys, 1988) and New Zealand earthquakes (Table 1). It can be seen that the curves agree where field observational data is most dense, whereas a discrepancy exists for smaller magnitude earthquakes (M_w < 6), for which field observational data is limited. Possible causes of this discrepancy are investigated as follows:

(1) The possibility exists that GMPEs in the near-field and/or for small magnitude earthquakes are inaccurate (e.g., Bommer et al., 2007). If GMPE estimates of a_{max} exceed instrumentally recorded values, then the framework illustrated in Fig. 4 will overestimate the maximum site-to-source distance at which liquefaction can be induced. Thus, the discrepancy between curves developed directly from liquefaction field observations and those back-calculated could be tied to the selected GMPE.

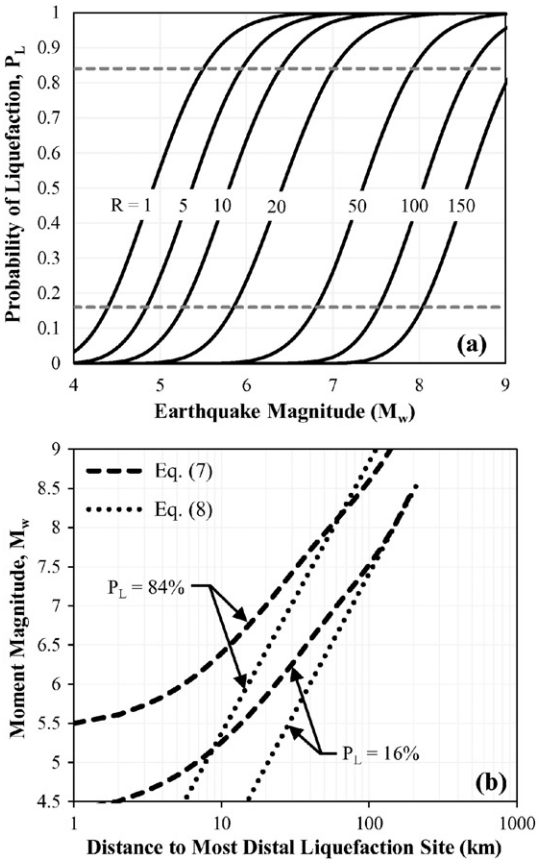

Fig. 8. (a) Probability of liquefaction vs. earthquake magnitude, as computed by Eq. (5) for select values of R_{jb}; (b) construction of probabilistic magnitude-bound curves for select probability of liquefaction (P_L) values (P_L = 16%; 84%), developed from probability curves computed by Eq. (5), shown in (a), and Eq. (6), not shown.

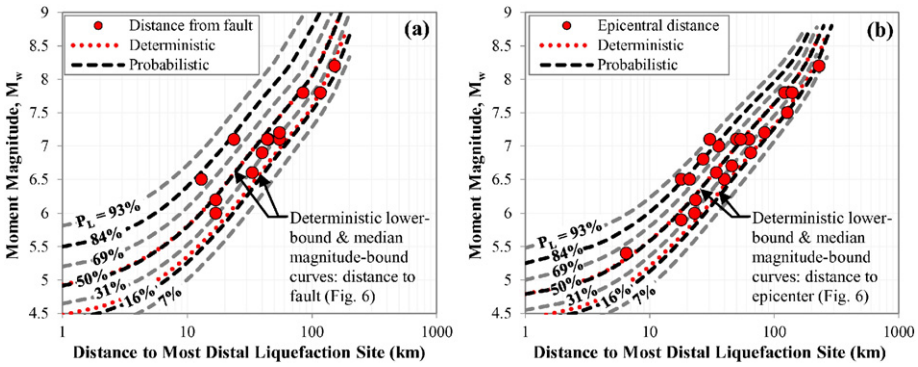

Fig. 9. Probabilistic back-calculated magnitude-bound relations for liquefaction probabilities (P_L) of 7%, 16%, 31%, 50%, 69%, 84%, and 93% (i.e., median ± 1.5σ prediction), where site-to-source distance is quantified in terms of (a) distance to fault (R_{jb}); and (b) epicentral distance (R_{epi}); also plotted is the database of New Zealand liquefaction observations (Table 1) and the deterministic lower-bound and median magnitude-bound curves developed previously (Fig. 6).

However, this seems unlikely since: (1) the Bradley (2010, 2013) GMPE provided predictions with sufficient accuracy in the 4 September 2010, M_W7.1 Darfield and 22 February 2011, M_w6.2 Christchurch earthquakes, independent of site-to-source distance (Bradley, 2013); (2) the small magnitude predictions needed to develop magnitude-bound curves are within the parameter space of the Bradley (2010, 2013) GMPE; and (3) it can be shown using numerous other GMPEs that similar discrepancies exist between back-calculated magnitude-bound curves and the field observational data shown in Fig. 10 for both New Zealand and global data.

(2) The possibility exists that estimates of FS_{liq} are erroneous for small magnitude earthquakes. In the liquefaction triggering framework used herein, the amplitude and duration of cyclic loading are respectively represented by a_{max} and MSF, where MSF is a function of M_w, amongst other factors. However, the relationship between M_w and MSF is uncertain for small magnitude events, and furthermore, many proposed MSFs do not account for potentially-significant variables (e.g., soil type, tectonic setting, and rupture-distance and -directivity) (e.g., Green and Terri, 2005; Green et al., 2008; Green and Lee, 2010; Carter et al., 2014). Thus, the discrepancy between curves developed directly from liquefaction field observations and those back-calculated could be tied to the selected MSF. A recent study has shown that MSF is a function of soil response (Boulanger and Idriss, 2014), which is not accounted for in the MSF inherent to the Cetin et al. (2004) liquefaction evaluation procedure. However, use of the Boulanger and Idriss (2014) liquefaction evaluation procedure only exacerbates the discrepancy between the curves. Thus, while the possibility persists that this discrepancy is related to magnitude-scaling, more research is required to develop MSFs that more fully account for soil response (e.g., Green and Terri, 2005; Lasley et al., 2015).

(3) It can be seen in Fig. 10 that magnitude-bound curves developed directly from liquefaction field observational data are subject to limitations in data. For example, only 15% of the earthquakes in the Ambraseys (1988) database are smaller than M_w6.0, whereas this percentage is even less for the New Zealand database. Amongst these limited cases, instances of high liquefaction susceptibility and/or greater than expected seismic loading may be lacking (i.e., conditions which increase the maximum distance to liquefaction). Since the curve developed from observational data is controlled by relatively few small-magnitude events, its position may inaccurately represent the range of possible outcomes. As such, as data is collected in future earthquakes having $M_w < 6$, better constraint of the magnitude-bound curves developed from observational data will result.

The discrepancy between curves for small magnitude earthquakes is believed to be unrelated to the focal mechanism and focal depth assumed in the development of the back-calculated curves, as evidenced by a limited parametric study.

Despite the uncertainty noted above for smaller magnitude events, the back-calculated magnitude-bound curves developed herein are recommended for analyses of paleoliquefaction evidence in New Zealand. Moreover, the probabilistic curves allow for the range of possible causative paleoearthquake magnitudes to be better understood and quantified. There are two principal ways in which these curves may be used, as described in the following. *First*, there are scenarios where multiple paleoliquefaction features are investigated, dated, mapped, and assigned to a common causative paleoearthquake, but historic records are incapable of suggesting how large the causative rupture may

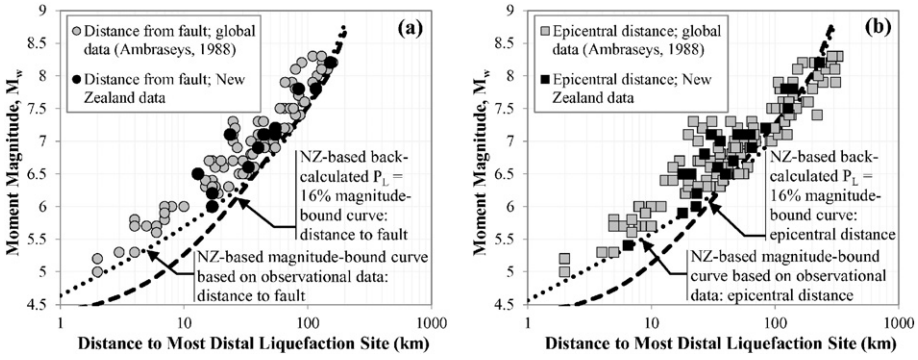

Fig. 10. Comparison of NZ-based magnitude-bound curves developed directly from field liquefaction observational data and back-calculated (P_L = 16%) using the simplified liquefaction evaluation procedure and a regionally applicable GMPE: (a) distance to fault (R_{jb}) and (b) epicentral distance (R_{epi}); data from historic global earthquakes (Ambraseys (1988)) and earthquakes in New Zealand (Table 1) are also plotted.

have been. For example, amongst several cases in the United States, Cox et al. (2007) delineated three paleoliquefaction fields in the southern Mississippi Embayment and proposed that one of these fields had a provisional maximum site-to-source distance of 23.5 km. While the commonly-used Ambraseys (1988) magnitude-bound curve estimates a magnitude of M_w6.0, the probabilistic curves developed herein give a more informative median ± σ estimate of M_w6.25 ± 0.45 for an equivalent liquefaction field in New Zealand. *Second*, there are scenarios in which an effort to determine the magnitude of an earthquake is aided by the historic and paleoseismic records, but is complicated by the existence of multiple possible causative earthquakes. For this scenario, which will be demonstrated herein, the probabilistic curves can be used to determine which earthquakes amongst a suite of possible events were more likely to have induced liquefaction at a particular site. In the following, the use of the back-calculated magnitude-bound curves is demonstrated by analyzing paleoliquefaction evidence recently discovered in Christchurch.

3. Demonstration of NZ-based magnitude-bound curves

Following the CES, a series of trenches were dug to investigate the structure and stratigraphy of modern, undisturbed liquefaction features (e.g., Green et al., 2012; Quigley et al., 2013). In some cases, trenching also uncovered evidence of paleoliquefaction within the subsurface. One such case is that of Sullivan Park in eastern Christchurch, a site of intensive investigations by Bastin et al. (2013, 2015). Here, oxidized, pre-CES liquefaction dikes were found to be cross-cut by lateral spreading fissures formed during the CES (e.g., Fig. 11). Cross-cutting relationships and ^{14}C dating indicate the causative earthquake most likely occurred between AD 1660–1803 and ca. 1905 (Bastin et al., 2015). Liquefaction was observed in the village of Kaiapoi, north of Christchurch, during the 1901 Cheviot earthquake (e.g., Berrill et al., 1994), however the Sullivan Park site provides the first evidence for pre-CES liquefaction in Christchurch. Thus, this discovery, along with others since (Tuttle et al., 2012; Villamor et al., 2014), provides the opportunity for paleoliquefaction evidence to help clarify the paleoseismic history of the region. For complete details of the Sullivan Park field investigation, and of the thorough efforts to date the paleoliquefaction feature, see Bastin et al. (2015).

As listed in Table 1, 8 earthquakes with documented liquefaction observations occurred in New Zealand between 1848 and 1930. An additional 4 events within or near the constrained timeframe (i.e., ca. 1660 to ca. 1905) affected the Canterbury region with the potential to induce liquefaction; these include the (1) 1870 ~M_w5.7 Lake Ellesmere earthquake (e.g., Downes and Yetton, 2012); (2) 1869 ~M_w4.8 Christchurch earthquake (e.g., Downes and Yetton, 2012); (3) 1717 ~M_w8.1 Alpine Fault earthquake (e.g., Sutherland et al., 2007); and (4) ca. 1400–1500~ M_w7.1 - M_w7.4 Porters Pass Fault earthquake (Howard et al., 2005). To investigate the possibility of these 12 earthquakes to have induced liquefaction in Sullivan Park, the magnitude and corresponding site-to-source distance are plotted in Fig. 12 along with the probabilistic magnitude-bound curves developed previously. For some of these events, paleoseismic studies have constrained the extents of fault rupture with reasonable accuracy. For example, Howard et al. (2005) mapped the Porters Pass Fault system extensively and proposed a history of recurrent earthquakes. Similarly, the extents of the 1717 Alpine Fault rupture are reasonably well-constrained by on-fault evidence, with a northern terminus likely near the Haupiri River (Sutherland et al., 2007; Berryman et al., 2012; De Pascale and Langridge, 2012). As discussed previously, the back-calculated magnitude-bound curves based on fault distance (i.e., R_{jb}) are derived directly from the framework established in this paper, whereas those based on R_{epi} are derived from the former using empirical conversions for site-to-source distance metrics proposed by Scherbaum et al. (2004). It is therefore recommended that the curves based on R_{jb} be used whenever possible. However, paleoliquefaction studies are often performed where faults do not manifest at the ground surface or are otherwise unknown. For pre-instrumental earthquakes, a macroseismic epicenter may be all that is known, whereas for pre-historical events, an "energy center" interpreted from liquefaction evidence could be the only indication of source region (Obermeier, 1996). For these cases, the magnitude-bound curves based on R_{epi} are likely more appropriate; for further discussion of this assumption and uncertainties relating to site-to-source distance metrics, see Green et al. (2005) and Olson et al. (2005b). Thus, for 4 events where the distance to fault rupture is reasonably well-constrained, the curves based on R_{jb} are used (Fig. 12a); for the remaining 8 events, the curves based on R_{epi} are used (Fig. 12b). The plotted distances in Fig. 12 are those from Sullivan Park to the fault ruptures (Fig. 12a) or epicenters (Fig. 12b). In addition, uncertainties are assigned to each M_w and site-to-source distance, as summarized in Table 2.

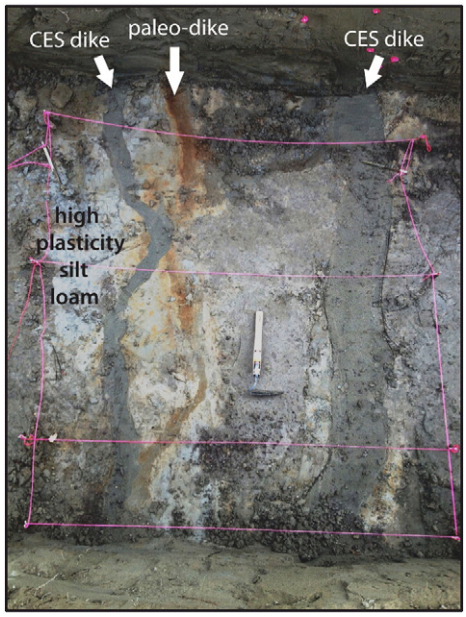

Fig. 11. Field photograph of liquefaction feeder dikes that formed during the 2010–2011 Canterbury earthquake sequence ('CES dike') and a paleoliquefaction feeder dike that formed between ca. 1660 and ca. 1905 A.D. Photograph taken of excavation floor, parallel to the ground surface, at ~1.2 m depth. Note similarity in morphology of CES dike on left side of image and paleo-dike (image after Bastin et al., 2015).

From Fig. 12, it can be seen that 7 of the 12 earthquakes considered plot below the P_L = 7% magnitude-bound curves, and as such, it is very unlikely that these events induced liquefaction in Sullivan Park. In addition, points plotting near the P_L = 16% curves suggest the occurrence of liquefaction that is marginal and isolated, rather than severe and widespread, where observations of the latter are more likely at site-to-source distances plotting well above the P_L = 50% magnitude-bound curves. As such, it is unlikely that any of the 12 events would induce liquefaction in Christchurch comparable to that observed in the largest events of the CES. For example, the fault rupturing in the M_w6.2 Christchurch earthquake was within 5 km of much of the Christchurch urban area, to include Sullivan Park; it can be seen in Fig. 12a that the corresponding magnitude-bound data would plot above the P_L = 93% curve. Possible causes of the paleoliquefaction in Sullivan Park are further investigated as follows:

- It can be seen in Fig. 12a that the ca. 1400–1500~ M_w7.1 - M_w7.4 Porter's Pass Fault earthquake (#1) plots just above the P_L = 16% curve and might thus have induced isolated, marginal liquefaction in Christchurch. However, since this event is believed to have occurred prior to the incidence of liquefaction in Sullivan Park (i.e., 1660 to 1905), it is likely not the causative earthquake.

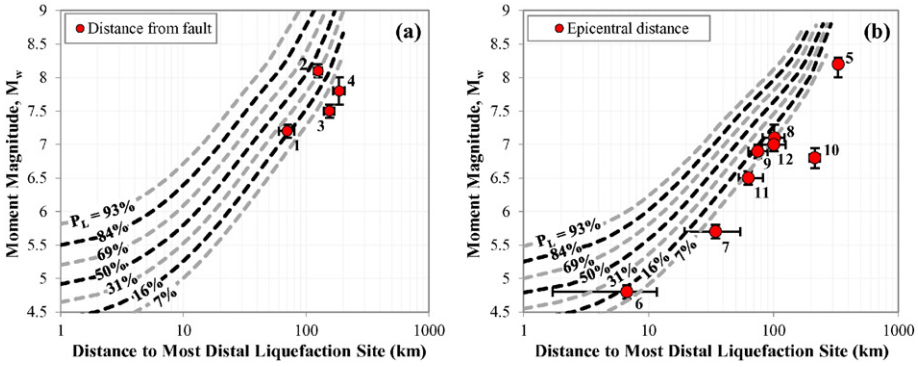

Fig. 12. Investigating the potential for 12 historical earthquakes to induce liquefaction at Sullivan Park using probabilistic back-calculated magnitude-bound curves, as described in the text. Events are parsed into (a) those with constrained rupture extents; and (b) those with an estimated epicenter only; all data is provided in Table 2.

- It can be seen in Fig. 12a that the 1717 ~M_w8.1 Alpine Fault earthquake (#2) plots between the P_L = 31% and P_L = 50% curves and might thus have induced liquefaction at Sullivan Park. It is speculated that the extent and severity of liquefaction in Christchurch would be far less than that observed during the largest events of the CES, but that sporadic marginal liquefaction might be expected.
- It can be seen in Fig. 12b that 3 events plot between the P_L = 7% and P_L = 16% curves: the 1869 ~M_w4.8 Christchurch earthquake (#6), 1888 ~M_w7.1 North Canterbury earthquake (#8), and 1901 ~M_w6.9 Cheviot earthquake (#9). While liquefaction was induced in Kaiapoi during the Cheviot earthquake, none was observed in the vicinity of Sullivan Park (~10 km further from the provisional epicenter), or anywhere else in Christchurch. As such, the Cheviot earthquake is unlikely the causative event, but the possibility exists that very marginal liquefaction was induced in Christchurch, but was not observed or documented. There is a minor possibility that the North Canterbury earthquake induced isolated and very marginal liquefaction in Christchurch, but the nearest observation was made in Hammer Springs, ~100 km from Sullivan Park (Fairless and Berrill, 1984). Lastly, and of most interest, is the 1869 Christchurch earthquake. While this event plots below the P_L = 16% curve, the uncertainty assigned to the source location by Downes and Yetton (2012) has important implications. Incorporating the uncertainty in epicenter location and M_w, the site-to-source distance for Sullivan Park could actually be closer to the P_L = 50% curve, and thus, similar to the 1717 Alpine Fault earthquake insofar as expected liquefaction at Sullivan Park. In addition, from analysis of CES aftershocks, Syracuse et al. (2013) delineated the previously unmapped North Christchurch Fault, shown in Fig. 13, and hypothesized that it was active prior to the CES (Syracuse et al., 2013). It can be seen in Fig. 13 that the epicenter of the 1869 earthquake proposed by Downes and Yetton (2012) falls near the surface projection of the proposed N. Christchurch Fault, which also encompasses Sullivan Park at its eastern boundary. While it can only be speculated that the 1869 rupture may have occurred on the N. Christchurch Fault, the findings of Syracuse et al. (2013) support the possibility that the site-to-source distance to Sullivan Park may have been less than the estimate of 6.7 km plotted in Fig. 12b.

In summary, while there are several possible causative events of the paleoliquefaction discovered by Bastin et al. (2015), the magnitude-bound curves developed herein suggest the 1869 ~M_w4.8 Christchurch or 1717 ~M_w8.1 Alpine Fault earthquakes are most likely amongst known earthquakes during the constrained time frame. In addition, it is suggested the Porters Pass Fault is capable of inducing liquefaction in Christchurch, with the severity dependent on the extent of fault rupture, which has shown to be variable (Howard et al., 2005). To these culpable earthquakes, we must add the possibility of strong earthquakes on other faults throughout the region (identified or unidentified) (e.g., Barnes et al., 2011; Dorn et al., 2010). To this end, the magnitude-bound curves based on R_{jb} indicate that $M_w \geq 6$ events within 12 km of the site, $M_w \geq 7$ events within 35 km of the site, and $M_w \geq 8$ events within 100 km of the site have $P_L \geq 50\%$. Within this realm, the Greendale Fault (i.e., the source of the 2010 M_w7.1 Darfield earthquake) is unlikely the cause of paleoliquefaction in Sullivan Park, since its central section is believed to have last ruptured ca. 20,000 to ca. 30,000 years ago (Hornblow et al., 2014). To determine the causative earthquake more definitively, there is a need for additional evidence at different distances from the provisional source locations, and/or having better-constrained ages from both paleoliquefaction deposits and paleo-earthquake fault ruptures. Nonetheless, it has been demonstrated that magnitude-bound curves can provide significant insight into past,

Table 2
Potential causative earthquakes of paleoliquefaction in Sullivan Park, Christchurch.

Year	Earthquake[a]	Estimated M_w	Plotted M_w	Estimated R_{epi} (km)[b]	Plotted R_{epi} (km)	Estimated R_{jb} (km)[c]	Plotted R_{jb} (km)	Reference
1400–1500	Porter's Pass[1]	7.1–7.3	7.2	–	–	60–80	70	Howard et al. (2005)
1717	Alpine Fault[2]	8.0–8.2	8.1	–	–	115–135	125	Sutherland et al. (2007)
1848	Marlborough[3]	7.4–7.6	7.5	–	–	140–170	155	Mason and Little (2006)
1929	Murchison[4]	7.6–8.0	7.8	–	–	166–206	186	Carr and Berrill (2004)
1855	Wairarapa[5]	8.0–8.3	8.2	311–351	331	–	–	GeoNet (2015)
1869	Christchurch[6]	4.7–4.9	4.8	1.7–11.7	6.7	–	–	Downes and Yetton (2012)
1870	L. Ellesmere[7]	5.6–5.8	5.7	19.4–54.4	34.4	–	–	Downes and Yetton (2012)
1888	N. Canterbury[8]	7.0–7.3	7.1	82–122	102	–	–	Doser and Robinson (2002)
1901	Cheviot[9]	6.8–7.0	6.9	62–90	75	–	–	Berrill et al. (1994)
1913	Westport[10]	6.65–6.95	6.8	185–235	215	–	–	Fairless and Berrill (1984)
1922	Motunau[11]	6.4–6.6	6.5	53–83	63	–	–	Doser and Robinson (2002)
1929	Arthur's Pass[12]	6.9–7.1	7.0	81–126	101	–	–	Doser and Robinson (2002)

[a] Numbers 1–12 indicate event identification, as labeled in Fig. 12
[b] Site-to-source distance from earthquake epicenter (R_{epi}) to Sullivan Park, Christchurch.
[c] Site-to-source distance from fault (R_{jb}) to Sullivan Park, Christchurch.

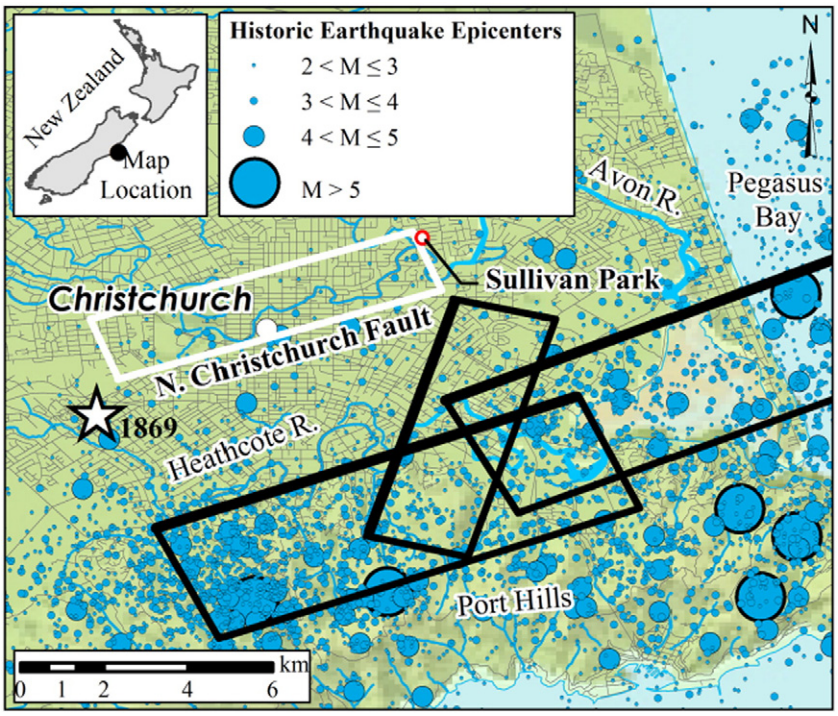

Fig. 13. Location of Sullivan Park in relation to: (1) modeled faults active in the Feb. 2011 Christchurch main shock (Beavan et al., 2013), as indicated by black rectangles with the bold line highlighting the up-dip edge of the fault; (2) the North Christchurch Fault, as proposed by Syracuse et al. (2013) using high-resolution relocation of CES aftershocks (indicated by a white rectangle); (3) historic earthquake epicenters (occurring through 8/2015) (GeoNet, 2015); and (4) the estimated epicenter of the 1869 Christchurch earthquake (indicated by a white star), as proposed by Downes and Yetton (2012).

present, and future hazards, even in cases where physical evidence is very limited.

4. Conclusions

To assist in the interpretation of paleoseismic histories, magnitude-bound curves are commonly used to estimate earthquake magnitudes from paleoliquefaction evidence. This study used two independent approaches to develop New Zealand based magnitude-bound curves: (1) using field observational data; and (2) using a back-calculation framework with the simplified liquefaction evaluation procedure and a regionally applicable GMPE, wherein both deterministic and probabilistic frameworks were used. These back-calculated curves are advantageous in that they may be developed for regions having limited or poorly documented field liquefaction observational data, and because soil- and site-specific conditions can be incorporated into magnitude-bound analyses. The proposed framework to develop back-calculated curves is thus a significant advancement. Moreover, probabilistic curves allow for the range of possible causative earthquake magnitudes to be better understood and quantified, and are therefore recommended. Provided in an electronic supplement are data for reproducing the probabilistic curves developed herein, which are intended for shallow crustal earthquakes with low Z_{tor} values; the user should recognize the limitations of applying these curves to deeper ruptures.

To demonstrate the use of the proposed magnitude-bound curves, paleoliquefaction investigated by Bastin et al. (2015) in eastern Christchurch was analyzed. The 1869 ~M_w4.8 Christchurch earthquake and/or 1717 ~M_w8.1 Alpine Fault earthquake are found to be the most likely candidates amongst known historical and paleoearthquakes for causing the paleoliquefaction between ca. 1660 and 1905 A.D. in Sullivan Park. This study demonstrated the potential of the proposed magnitude-bound curves to provide insight into past, present, and future hazards, proving their utility even in cases of limited evidence. When additional paleoliquefaction is discovered in New Zealand, the curves developed herein will aid in more accurately assessing regional seismic hazards. And, from a more global perspective, the approaches to develop and use magnitude bound curves proposed herein are not limited to New Zealand, but rather, can be applied worldwide.

Acknowledgments

This study is based on work supported by the U.S. National Science Foundation (NSF) grants CMMI-0962952, CMMI-1407428 and CMMI-1435494, and US Geological Survey (USGS) grants G12AP20002 and G14AP00046. However, any opinions, findings, and conclusions or recommendations expressed in this paper are those of the authors and do not necessarily reflect the views of NSF or USGS. The authors also gratefully acknowledge the input from Professor Adrian Rodriguez-Marek at Virginia Tech on computing probabilistic, back-calculated magnitude bound curves, and review comments by Drs. Stephen Obermeier and Tish Tuttle.

Appendix A. Supplementary data

Supplementary data to this article can be found online at http://dx.doi.org/10.1016/j.enggeo.2015.08.023.

References

Almond, P., Villamor, P., Tuttle, M., Langridge, R.M., Clark, K., Eger, A., Bastin, S., Quigley, M., Barker, P., Vandergoes, M., 2012. Liquefaction induced by the 2010–2011 Canterbury earthquake sequence and implications of recently discovered paleoliquefaction features. Geol. Soc. Am. Abstr. Programs 44 (7), 414.

Ambraseys, N.N., 1988. Engineering seismology. Earthq. Eng. Struct. Dyn. 17, 1–105.

Anderson, H., Beanland, S., Buck, G., Darby, D., Downes, G., Haines, J., Jackson, J., Robinson, R., Webb, T., 1994. The 1968 may 23 Inangahua, New Zealand, earthquake: an integrated geological, geodetic, and seismological source model. N. Z. J. Geol. Geophys. 37 (1), 59–86.

Andrus, R.D., Stokoe, K.H., 2000. Liquefaction resistance of soils from shear-wave velocity. J. Geotech. Geoenviron. 126 (11), 1015–1025.

Aydan, O., Ulusay, R., Kumsar, H., Tuncay, E., 2000. Site investigation and engineering evaluation of the Duzce-Bolu earthquake of November 12, 1999. Turkish Earthquake Foundation, Istanbul (Report No. TDV/DR 09-51, 307 pp.).

Barnes, P.M., Castellazzi, C., Gorman, A., Wilcox, S., 2011. "Submarine Faulting Beneath Pegasus Bay, Offshore Christchurch. Report WLG2011-28. National Institute of Water and Atmospheric Research Ltd (NIWA), Wellington, New Zealand.

Bastin, S., Quigley, M., Bassett, K., 2015. Paleo-liquefaction in Christchurch, New Zealand. Bull. Geol. Soc. Am. http://dx.doi.org/10.1130/B31174.1.

Bastin, S.H., Quigley, M., Bassett, K., Green, R.A., 2013. Characterisation of Modern and Paleo-Liquefaction Features in Eastern Christchurch, NZ Following the 2010–12 Canterbury Earthquake Sequence. In: Chin, C.Y. (Ed.), Proc. 19th New Zealand Geotechnical Society (NZGS 2013) Symposium – Infrastructure, Lifelines, and Natural Disasters (Queenstown, New Zealand, 20–22 November).

Beavan, J., Motagh, M., Fielding, E.J., Donnelly, N., Collett, D., 2012. Fault slip models of the 2010–2011 Canterbury, New Zealand, earthquakes from geodetic data and observations of postseismic ground deformation. N. Z. J. Geol. Geophys. 55 (3), 207–221.

Benn, J.L., 1992. A review of earthquake hazards on the West Coast. The West Coast Regional Council, Greymouth, New Zealand.

Berg, G.V., Bolt, B.A., Sozen, M.A., Rjahn, C., 1980. Earthquake in Romania — March 4, 1977: An Engineering Report. National Research Council and Earthquake Engineering Research Institute, National Academy Press, Washington D.C. (39 pp.).

Berrill, J.B., Mulqueen, P.C., Ooi, E.T.C., 1994. Liquefaction at Kaiapoi in the 1901 cheviot, New Zealand, earthquake. Bull. N. Z. Natl. Soc. Earthq. Eng. 27 (3), 178–189.

Berryman, K., Cooper, A., Norris, R., Villamor, P., Sutherland, T.W., Schermer, E., Langridge, R., Biasi, G., 2012. Late Holocene rupture history of the alpine fault in south Westland, New Zealand. Bull. Seismol. Soc. Am. 102 (2), 620–638.

Bommer, J.J., Stafford, P.J., Alarcon, J.E., Akkar, S., 2007. The influence of magnitude range on empirical ground-motion prediction. Bull. Seismol. Soc. Am. 97 (6), 2152–2170.

Boore, D.M., 2011. In: Akkar, S., Gulkan, P., van Eck, T. (Eds.), Ground-motion prediction equations (GMPEs) from a global dataset: the PEER NGA equationsEarthquake Data in Engineering Seismology 14. Springer, Netherlands, pp. 3–15 (276 pp.).

Boulanger, R.W., Idriss, I.M., 2012. Probabilistic standard penetration test-based liquefaction-triggering procedure. J. Geotech. Geoenviron. 138 (10), 1185–1195.

Boulanger, R.W., Idriss, I.M., 2014. CPT and SPT based liquefaction triggering procedures. Report No. UCD/CGM-14/01. Department of Civil and Environmental Engineering, University of California at Davis, USA.

Bradley, B.A., 2010. NZ-specific pseudo-spectral acceleration ground motion prediction equations based on foreign models. Department of Civil and Natural Resources Engineering, University of Canterbury, Christchurch, New Zealand (324 pp.).

Bradley, B.A., 2013. A New Zealand-specific pseudo-spectral acceleration ground-motion prediction equation for active shallow crustal earthquakes based on foreign models. Bull. Seismol. Soc. Am. 103 (3), 1801–1822.

Carr, K., Berrill, J., 2004. "Liquefaction Case Histories from the West Coast of the South Island, New Zealand.". Research Report 2004–04. Department of Civil Engineering, University of Canterbury, Christchurch, New Zealand.

Carter, W.L., Green, R.A., Bradley, B.A., Cubrinovski, M., 2014. The Influence of Near-Fault Motions on Liquefaction Triggering during the Canterbury Earthquake Sequence. In: Orense, R.P., Towhata, I., Chouw, N. (Eds.), Soil Liquefaction During Recent Large-Scale Earthquakes. CRC Press, Leiden, The Netherlands, pp. 57–68.

Castilla, R.A., Audemard, F.A., 2007. Sand blows as a potential tool for magnitude estimation of pre-instrumental earthquakes. J. Seismol. 11, 473–487.

Cetin, K.O., Seed, R.B., Der Kiureghian, A., Tokimatsu, K., Harder, L.F., Kayen, R.E., Moss, R.E.S., 2004. Standard penetration test-based probabilistic and deterministic assessment of seismic soil liquefaction potential. J. Geotech. Geoenviron. Eng. ASCE 130 (12), 1314–1340.

CGD — Canterbury Geotechnical Database, 2012. Aerial Photography Map Layer CGD0100 — 1 June 2012, retrieved [12/12] from https://canterburygeotechnicaldatabase.projectorbit.com.

Chiou, B.S.-J., Youngs, R.R., 2008. An NGA model for the average horizontal component of peak ground motion and response spectra. Earthq. Spectra 24, 173–216.

Christensen, S.A., Mar 2001. Regional Liquefaction Study for Waimakariri District. Proceedings of the New Zealand Society of Earthquake Engineering 2001 Technical Conference. New Zealand Society of Earthquake Engineering, Taupo NZ, pp. 23–25.

Cox, R.T., Larsen, D., Forman, S.L., Woods, J., Morat, J., Galluzzi, J., 2004. Preliminary assessment of sand blows in the southern Mississippi embayment. Bull. Seismol. Soc. Am. 93 (3), 1125–1142.

Cox, R.T., Hill, A.A., Larsen, D., Holzer, T., Forman, S.L., Noce, T., Gardner, C., Morat, J., 2007. Seismotectonic implications of sand blows in the southern Mississippi embayment. Eng. Geol. 89, 278–299.

Darendeli, M.B., 2001. Development of a new family of normalized modulus reduction and material damping curves PhD Dissertation University of Texas at Austin, Austin, TX USA.

De Lange, W.P., Healy, T.R., 1986. New Zealand tsunamis 1840–1982. N. Z. J. Geol. Geophys. 29, 115–134.

De Pascale, G.P., Langridge, R.M., 2012. New on-fault evidence for a great earthquake in A.D. 1717, central alpine fault, New Zealand. Geology 40 (9), 791–794.

Dobry, R., Ladd, R.S., Yokel, F.Y., Chung, R.M., Powell, D., 1982. Prediction of pore water pressure buildup and liquefaction of sands during earthquakes by the cyclic strain method, NBS Building Science Series 138. US Department of Commerce (152 pp.).

Dobry, R., Powell, D.J., Yokel, F.Y., Ladd, R.S., 1980. Liquefaction potential of saturated sand — the stiffness method. Proceedings of the 7th World Conference on Earthquake Engineering, Istanbul 3, pp. 25–32.

Dorn, C., Green, A.G., Jongens, R., Carpentier, S., Kaiser, A.E., Campbell, F., Finnemore, M., Pettinga, J., 2010. High -resolution seismic images of potentially seismogenic structures beneath the northwest Canterbury plains, New Zealand. J. Geophys. Res. 115 (B11).

Doser, D.I., Robinson, R., 2002. Modeling stress chanfes induced by earthquakes in the southern Marlborough region, south island, New Zealand. Bull. Seismol. Soc. Am. 92 (8), 3229–3238.

Downes, G., Yetton, M., 2012. Pre-2010 historical seismicity near Christchurch, New Zealand: the 1869 M_w4.7–4.9 Christchurch and 1870 M_w5.6–5.8 lake Ellesmere earthquakes. N. Z. J. Geol. Geophys. 55 (3), 199–205.

Dowrick, D.J., Smith, E.G.C., 1990. Surface wave magnitudes of some New Zealand earthquakes 1901–1988. Bull. N. Z. Natl. Soc. Earthq. Eng. 23, 198–210.

Fairless, G., Berrill, J., 1984. Liquefaction during historic earthquakes in New Zealand. Bull. N. Z. Soc. Earthq. Eng. 17, 280–291.

Franks, C.A., 1988. Engineering geological aspects of the edgecomb, New Zealand earthquake of 2 March 1987. Q. J. Eng. Geol. 21, 337–345.

Galli, P., 2000. New empirical relationships between magnitude and distance for liquefaction. Tectonophysics 324, 169–187.

GeoNet (2015). "New Zealand earthquake occurrence data: felt quakes." <http://geonet.org.nz/> (Aug. 21 2015).

Glassey, P.J., 2006. Geological hazards: Southland district council lifelines study. GNS Science Consultancy Report 2006/100. GNS Science Research Centre, Dunedin New Zealand.

Geotechnical Reconnaissance of the 2010 Darfield (New Zealand) earthquake. In: Green, R.A., Cubrinovski, M. (Eds.), Report of the National Science Foundation-Sponsored Geotechnical Extreme Events Reconnaissance (GEER) Team, GEER Association Report No. GEER-024.

Green, R.A., Lee, J., 2010. The influence of near-fault rupture directivity on liquefaction. Proc. Ninth US National and Tenth Canadian Conf. on Earthquake Engineering, Toronto, Canada, 25–29 July 2010.

Green, R.A., Olson, S.M., 2015. Interpretation of liquefaction field case histories for use in developing liquefaction triggering curves. Proc. 6th International Conference on Earthquake Geotechnical Engineering (6ICEGE), Christchurch, New Zealand, 2–4 November (in press).

Green, R.A., Terri, G.A., 2005. Number of Equivalent Cycles Concept for Liquefaction Evaluations - Revisited. J. Geotech. Geoenviron. 131 (4), 477–488.

Green, R.A., Cubinovski, M., Cox, B., Wood, C., Wotherspoon, L., Bradley, B., Maurer, B.W., 2014. Select liquefaction case histories from the 2010–2011 Canterbury earthquake sequence. Earthq. Spectra 30 (1), 131–153.

Green, R.A., Lee, J., White, T.M., Baker, J.W., 2008. The Significance of Near-Fault Effects on Liquefaction. Proc. 14th World Conf. on Earthquake Engineering, Paper No. S26-019.

Green, R.A., Maurer, B.W., Bradley, B.A., Wotherspoon, L., Cubrinovski, M., 2013. Implications from Liquefaction Observations in New Zealand for Interpreting Paleoliquefaction Data in the Central-Eastern United States (CEUS). Final Technical Report Award No. G12AP20002. U.S. Geological Survey, Reston, VA.

Green, R.A., Maurer, B.W., Wotherspoon, L., Cubrinovski, M., Quigley, M., Bastin, S., 2012. Use of liquefaction observations in New Zealand for interpreting paleoliquefaction features in the NMSZ. Seismol. Res. Lett. 84 (1), 153.

Green, R.A., Olson, S.M., Obermeier, S.F., 2005. Geotechnical analysis of paleoseismic shaking using liquefaction effects: field examples. Eng. Geol. 76, 263–293.

Hancox, G.T., 2005. Landslides and liquefaction effects caused by the 1855 Wairarapa earthquake: then and now. In: Townend, J., Langridge, R., Jones, A. (Eds.), The 1855 Wairarapa Earthquake Symposium: 150 years of thinking about magnitude 8+ earthquakes and seismic hazard in New Zealand. Greater Wellington Regional Council.

Hancox, G.T., Dellow, G., Mc Saveney, B., Villamor, P., 2004. Reconnaissance studies of landslides caused by the ML 5.4 Lake Rotoehu earthquake and swarm of July 2004. Institute of Geological & Nuclear Sciences Science report 2004/24 (21 pp.).

Hornblow, S., Quigley, M., Nicol, A., Van Dissen, R., Wang, N., 2014. Paleoseismology of the 2010 Mw 7.1 Darfield (Canterbury) earthquake source, Greendale fault, New Zealand. Tectonophysics 637, 178–190.

Howard, M., Nicol, A., Campbell, J., Pettinga, J.R., 2005. Holocene paleoearthquakes on the strike-slip Porters Pass Fault, Canterbury, New Zealand. N. Z. J. Geol. Geophys. 48, 59–74.

Idriss, I.M., Boulanger, R.W., 2008. Soil liquefaction during earthquakes. Monograph MNO-12. Earthquake Engineering Research Institute, Oakland, CA (261 pp.).

Ishibashi, I., Zhang, X.J., 1993. Unified dynamic shear moduli and damping ratios of sand and clay. Soils Found. 33 (1), 182–191.

Kam, W.Y., Akguzel, U., Pampanin, S., 2011. 4 weeks on: preliminary reconnaissance report from the Christchurch 22 Feb 2011 6.3M_w earthquake. Report, New Zealand Society of Earthquake Engineering, Wellington, New Zealand.

Kayen, R., Moss, R.E.S., Thompson, E.M., Seed, R.B., Cetin, K.O., Der Kiureghian, A., Tanaka, Y., Tokimatsu, K., 2013. Shear-wave velocity-based probabilistic and deterministic assessment of seismic soil liquefaction potential. J. Geotech. Geoenviron. 139 (3), 407–419.

Kuribayahsi, E., Tatsuoka, F., 1975. Brief review of liquefaction during earthquakes in Japan. Soils Found. 15 (4), 81–92.

Lasley, S., Green, R.A., Rodriguez-Marek, A., 2015. Number of equivalent stress cycles for liquefaction evaluations in active tectonic and stable continental regimes. Journal of Geotechnical and Geoenvironmental Engineering (in press).

Mackey, B.H., Quigley, M.C., 2014. "Strong proximal earthquakes revealed by cosmogenic ^{3}He dating of prehistoric rockfalls, Christchurch, New Zealand. Geology 42 (11), 975–978.

Mason, D.P.M., Little, T.A., 2006. Refined slip distribution and moment magnitude of the 1848 Marlborough earthquake, Awatere fault, New Zealand. N. Z. J. Geol. Geophys. 49 (3), 375–382.

Maurer, B.W., Green, R.A., Bradley, B.A., Cubrinovski, M., 2014. Assessment of aging correction factors for liquefaction resistance at sites of recurrent liquefaction. 10th National Conference on Earthquake Engineering, July 20–26, Anchorage Alaska. Network for Earthquake Engineering Simulation (distributor) http://dx.doi.org/10.4231/D3B27PR92 (10 pp.).

Moss, R.E.S., Seed, R.B., Kayen, R.E., Stewart, J.P., Der Kiureghian, A., Cetin, K.O., 2006. CPT-based probabilistic and deterministic assessment of in situ seismic soil liquefaction potential. J. Geotech. Geoenviron. Eng. ASCE 132 (8), 1032–1051.

Obermeier, S.F., 1996. Using liquefaction-induced features for paleoseismic analysis. In: McCalpin, J.P. (Ed.), Paleoseismology. Academic Press, San Diego, CA, pp. 331–396.

Obermeier, S.F., 1998. Liquefaction evidence for strong earthquakes of Holocene and latest Pleistocene ages in the states of Indiana and Illinois, USA. Eng. Geol. 50, 227–254.

Obermeier, S.F., Dickenson, S.E., 2000. Liquefaction evidence for the strength of ground motions resulting from the late Holocene Cascadia subduction earthquakes, with emphasis on the event of 1700 A.D. Bull. Seismol. Soc. Am. 90 (4), 876–896.

Obermeier, S.F., Olson, S.M., Green, R.A., 2005. Field occurrences of liquefaction-induced features: a primer for engineering and geologic analysis of paleoseismic shaking. Eng. Geol. 76, 209–234.

Obermeier, S.F., Pond, E.C., Olsen, S.M. with contributions by Green, R.A., Mitchell, J.K., and Stark, T.D. (2001). "Paleoliquefaction studies in continental settings: geologic and geotechnical factors in interpretations and back-analysis." U.S. Geological Survey Open-File Report 01–029.

Olson, S.M., Green, R.A., Obermeier, S.F., 2005a. Geotechnical analysis of paleoseismic shaking using liquefaction features: a major updating. Eng. Geol. 76, 235–261.

Olson, S.M., Green, R.A., Obermeier, S.F., 2005b. Revised magnitude bound relation for the Wabash valley seismic zone of the central United States. Seismol. Res. Lett. 76 (6), 756–771.

Papadopoulos, G.A., Lefkopoulos, 1993. Magnitude-distance relations for liquefaction in soil from earthquakes. Bull. Seismol. Soc. Am. 83 (3), 925–938.

Papathanassiou, G., Pavlides, S., Christaras, B., Pitilakis, K., 2005. Liquefaction case histories and empirical relations of earthquake magnitude versus distance from the broader Aegean region. J. Geodyn. 40, 257–278.

Parker, M and Steenkamp, D. (2012). "The economic impact of the Canterbury earthquakes." Reserve Bank of New Zealand: Bulletin 75(3): 13–25.
Pirrotta, C., Barbano, M.S., Guarnieri, P., Gerardi, F., 2007. A new dataset and empirical relationships between magnitude/intensity and epicentral distance for liquefaction in central-eastern Sicily. Ann. Geophys. 50(6), 763–774.
Quigley, M., Bastin, S., Bradley, B., 2013. Recurrent liquefaction in Christchurch, New Zealand during the Canterbury earthquake sequence. Geology 41 (4), 419–422.
Reyners, M., McGinty, P., Cox, S., Turnbull, I., O'Neill, T., Gledhill, K., Hancox, G., Beavan J., Matheson, D., McVerry, G., Cousins, J., Zhao, J., Cowan, H., Caldwell, G., Bennie, S., the GeoNet team. (2003). "The M_w7.2 Fiordland earthquake of August 21, 2003: background and preliminary results." Bull. N. Z. Soc. Earthq. Eng., 36(4): 233–248.
Rix, G.J., Stokoe, K.H., 1991. Correlation of initial tangent modulus and cone penetration resistance. In: Huang, A.B. (Ed.), Calibration Chamber TestingInternational Symposium on Calibration Chamber Testing. Elsevier Publishing, New York, pp. 351–362.
Robertson, P.K., Wride, C.E., 1998. Evaluating cyclic liquefaction potential using cone penetration test. Can. Geotech. J. 35 (3), 442–459.
Scherbaum, F., Schmedes, J., Cotton, F., 2004. On the conversion of source-to-site distance measures for extended earthquake source models. Bull. Seismol. Soc. Am. 94 (3), 1053–1069.
Seed, H.B., DeAlba, P., 1986. Use of the SPT and CPT tests for evaluating the liquefaction resistance of sands. Use of in-situ Tests in Geotechnical Engineering, ASCE Geotechnical Special Publication 6, pp. 281–302.
Seed, H.B., Idriss, I.M., 1971. Simplified procedure for evaluating soil liquefaction potential. J. Soil Mech. Found. Div. ASCE 97 (9), 1249–1273.
Seed, H.B., Tokimatsu, K., Harder, L.F., Chung, R.M., 1985. Influence of SPT procedures in soil liquefaction resistance evaluations. J. Geotech. Eng. Div. ASCE 111 (2), 1425–1445.
Seed, H.B., Wong, R.T., Idriss, I.M., Tokimatsu, K., 1986. Moduli and damping factors for dynamic analyses of cohesionless soils. J. Geotech. Geoenviron. 112 (GT11), 1016–1032.
Stark, T.D., Olson, S.M., 1995. Liquefaction resistance using CPT and field case histories. J. Geotech. Eng. ASCE 121 (12), 856–869.
Stirling, M., Litchfield, N., Smith, W., Barnes, P., Gerstenberger, M., McVerry, G., Pettinga, J., 2007. Updated probabilistic seismic hazard assessment for the Canterbury region. Environment Canterbury Report No. U06/6.
Stirling, M., Yetton, M., Pettinga, J., Berryman, K., Downes, G., 1999. Probabilistic seismic hazard assessment and earthquake scenarios for the Canterbury region, and historic earthquakes in Christchurch: stage 1 (part b) of Canterbury regional council's earthquake hazard and risk assessment study. IGNS Report U99/18.
Sutherland, R, Eberhart-Phillips, D., Harris, R.A., Stern, T.A., Beavan, R.J., Ellis, S.M., Henrys, S.A., Cox, S.C., Norris, R.J., Berryman, K.R., Townend, J., Bannister, S.C., Pettinga, J., Leitner, B., Wallace, L.M., Little, T.A., Cooper, A.F., Yetton, M., and Stirling, M.W. (2007). "Do great earthquakes occur on the Alpine Fault in central South Island, New Zealand?" p. 235–251 in: Okaya, D.A.; Stern, T.A.; Davey, F.J. (eds) A continental plate boundary: tectonics at South Island, New Zealand. Washington, DC: American Geophysical Union. Geophysical monograph 175.
Syracuse, E.M., Thurber, C.H., Rawles, C.J., Savage, M.K., Bannister, S., 2013. High-resolution relocation of aftershocks of the M_w7.1 Darfield, New Zealand, earthquake and implications for fault activity. J. Geophys. Res. 118 (8), 4184–4195.
Talwani, P., Schaeffer, W.T., 2001. Recurrence rates of large earthquakes in the South Carolina coastal plain based on paleoliquefaction data. J. Geophys. Res. 106, 6621–6642.
Towhata, I., Maruyama, S., Kasuda, K., Koseki, J., Wakamatsu, K., Kiku, H., Kiyota, T., Yasuda, S., Taguchi, Y., Aoyama, S., Hayashida, T., 2014. Liquefaction in the Kanto region during the 2011 off the pacific coast of Tohoku earthquake. Soils Found. 54 (4), 859–873.
Tuttle, M.P., Hartleb, R., 2012. Appendix E: Central and Eastern U.S. paleoliquefaction database, uncertainties associated with paleoliquefaction data, and guidance for seismic source characterization, in the Central and Eastern U.S. Seismic Source Characterization for Nuclear Facilities, Technical Report, EPRI, Palo Alto, CA, U.S. DOE, and U.S. NRC, 135 p. plus database.
Tuttle, M.P., 2001. The use of liquefaction features in paleoseismology: lessons learned in the new Madrid seismic zone, central United States. J. Seismol. 5, 361–380.
Tuttle, M., Villamor, P., Almond, P., 2012. Paleoliquefaction lessons learned from the 2010–2011 Canterbury, New Zealand, earthquakes. Geol. Soc. Am. Abstr. Programs 44 (7), 302.
Tuttle, M.P., Dyer-Williams, K., Barstow, N.L., 2002a. Paleoliquefaction study of the Clarendon-Lindon fault system, western New York state. Tectonophysics 353, 263–286.
Tuttle, M.P., Schweig, E.S., Campbell, J., Thomas, P.M., Sims, J.D., Lafferty, R.H., 2005. Evidence for new Madrid earthquakes in A.D. 300 and 2350 B.C. Seismol. Res. Lett. 76, 489–501.
Tuttle, M.P., Schweig, E.S., Sims, J.D., Lafferty, R.H., Wolf, L.W., Haynes, M.L., 2002b. The earthquake potential of the new Madrid seismic zone. Bull. Seismol. Soc. Am. 92 (6), 2080–2089.
Van Dissen, R., McSaveney, M., Townsend, D., Hancox, G., Little, T.A., Ries, W., Perrin, N., Archibald, G., Dellow, G., Massey, C., Misra, S., 2013. Landslides and liquefaction generated by the Cook Strait and Lake Grassmere earthquakes: a reconnaissance report. Bull. N. Z. Soc. Earthq. Eng. 46 (4), 196–200.
Villamor, P., Giona-Bucci, M., Almond, P., Tuttle, M., Langridge, R., Clark, K., Ries, W., Vandergoes, M., Barker, P., Martin, F., Bastin, S., Watson, M., Howarth, J., Quigley, M., 2014. Exploring methods to assess paleoliquefaction in the Canterbury area. GNS Science Consultancy Report 2014/183. GNS Science, Lower Hutt New Zealand (142 pp.).
Wakamatsu, K., 1993. History of Soil Liquefaction in Japan and Assessment of Liquefaction Potential Based on Geomorphology. A Thesis in the Department of Architecture Presented in Partial Fulfillment of the Requirements for the Degree of Doctor of Engineering. Waseda University, Tokyo, Japan.
Whitman, R.V., 1971. Resistance of soil to liquefaction and settlement. Soils Found. 11 (4), 59–68.
Wood, C.M., Cox, B.R., Wotherspoon, L.M., Green, R.A., 2011. Dynamic site characterization of Christchurch strong motion stations. Bull. N. Z. Soc. Earthq. Eng. 44 (4), 195–204.
Wotherspoon, L., Orense, R., Bradley, B.A., Cox, B., Green, R.A., Wood, C., 2014. Soil profile characterization of Christchurch strong motion stations. Proc. 10th National Conference on Earthquake Engineering (10NCEE), Anchorage, AK, 21–25 July.
Youd, T.L., Hoose, S.N., 1977. Liquefaction susceptibility and geologic setting. Proceedings of the 6th World Conference on Earthquake Engineering, New Delhi, India 3, pp. 2189–2194.
Youd, T.L., Perkins, D.M., 1978. Mapping liquefaction-induced ground failure potential. J. Geotech. Eng. Div. 104, 433–446.
Youd, T.L., Idriss, I.M., Andrus, R.D., Arango, I., Castro, G., Christian, J.T., Dobry, R., Finn, W.D.L., Harder, L.F., Hynes, M.E., Ishihara, K., Koester, J.P., Liao, S.S.C., Marcuson, W.F., Martin, G.R., Mitchell, J.K., Moriwaki, Y., Power, M.S., Robertson, P.K., Seed, R.B., Stokoe, K.H., 2001. Liquefaction resistance of soils: summary report from the 1996 NCEER and 1998 NCEER/NSF workshops on evaluation of liquefaction resistance of soils. J. Geotech. Geoenviron. 127 (4), 297–313.